Symbol-Scaling based Interference Exploitation in ISAC Systems: From Symbol Level to Block Level

Yiran Wang, Xiaoyan Hu, *Member, IEEE*, Ang Li, *Senior Member, IEEE*,
Christos Masouros, *Fellow, IEEE*, Kai-Kit Wong, *Fellow, IEEE*, Kun Yang, *Fellow, IEEE*

***Abstract*—In this paper, we investigate the constructive interference (CI) based symbol-level precoding (SLP) design for integrated sensing and communication (ISAC) systems, where a multi-antenna base station (BS) serves multiple single-antenna communication users while simultaneously detecting targets of interest. Specifically, the minimum communication CI scaling factor among the users is maximized under radar performance constraint and power constraint. In order to solve the proposed optimization problem, two groups of approximate feasible domains are adopted to transform the optimization problem into convex. In order to improve the efficiency of the proposed precoding scheme, we adopt a modified Hooke-Jeeves pattern search algorithm for the convex subproblems. We further propose a weighted optimization scheme which considers the tradeoff between radar performance and communication performance as the objective function. By analyzing the Lagrangian function and Karush-Kuhn-Tucker (KKT) condition of the weighted optimization problem, we formulate the corresponding dual problem, which is a simple quadratic programming (QP) problem and can be easily solved. In addition, we further extend the proposed CI precoding scheme from symbol level to block level, in order to be more consistent with the currently used communication systems and achieve better ISAC performance. Extensive simulation results are provided to demonstrate the advantages and the effectiveness of the proposed symbol-scaling based CI-SLP design and CI-based block-level precoding (CI-BLP) design in ISAC systems.**

***Index Terms*—Integrated sensing and communication (ISAC), constructive interference (CI), symbol-level precoding (SLP), block-level precoding (BLP), symbol scaling.**

Manuscript received 17 May, 2024; revised 02 October, 2024; accepted 18 December, 2024. The work of Xiaoyan Hu was supported in part by the National Natural Science Foundation of China (NSFC) under Grants 62201449, 62471380, in part by the Young Elite Scientists Sponsorship Program by CAST under Grant No.YESS20230611, in part by the Key R&D Projects of Shaanxi Province under Grant 2023-YBGY-040, in part by the open research fund of National Mobile Communications Research Laboratory, Southeast University (No. 2025D08), in part by the Qin Chuang Yuan High-Level Innovation and Entrepreneurship Talent Program under Grant QCYRCXM-2022-231, and in part by the "Si Yuan Scholar" Foundation. The work of Ang Li was supported in part by the Young Elite Scientists Sponsorship Program by CIC (Grant No. 2021QNRC001), in part by the National NSFC under Grants 62101422, 62371386, in part by the Science and Technology Program of Shaanxi Province under Grant 2024JC-JCQN-59, in part by the open research fund of National Mobile Communications Research Laboratory, Southeast University (No. 2024D01), and in part by the Xiaomi Young Scholars Program. The work of Kun Yang was supported in part by National NSFC (No. 62132004), and the Municipal Government of Quzhou (Grant No.: 2023D005). An earlier version of this paper was presented in part at the IEEE/CIC International Conference on Communications in China (ICCC), Hangzhou, China, August 2024. The associate editor coordinating the review of this article and approving it for publication was Prof. L. Liu. *(Corresponding author: Xiaoyan Hu.)*

Y. Wang is with the School of Information and Communications Engineering, Faculty of Electronic and Information Engineering, Xi'an Jiaotong University, Xi'an 710049, China. (e-mail: yiranwang@stu.xjtu.edu.cn).

X. Hu and A. Li are with the School of Information and Communications Engineering, Faculty of Electronic and Information Engineering, Xi'an Jiaotong University, Xi'an 710049, China, and also with the National Mobile Communications Research Laboratory, Southeast University, Nanjing 210096, China. (e-mail: {xiaoyanhu, ang.li.2020}@xjtu.edu.cn).

C. Masouros and K.-K. Wong are with the Department of Electronic and Electrical Engineering, University College London, London WC1E 7JE, U.K. (e-mail: {c.masouros, kai-kit.wong}@ucl.ac.uk).

K. Yang is with the School of Computer Science and Electronic Engineering, University of Essex, Colchester CO4 3SQ, U.K. (e-mail: kunyang@essex.ac.uk).

I. Introduction

With the rapid growth of wireless services, spectrum resources are becoming increasingly scarce. The radar frequency bands have a large portion of the available spectrum that is promising to be shared with various communication systems. Spectrum sharing between radar and communication systems is consistent with the continuous fusion of integrated sensing and communication (ISAC) [1]–[5], which has triggered massive research on coexistence, cooperation and joint design of these two functions [6]–[9].

Previous works on joint radar-communication design mainly focuses on: 1) radar-communication coexistence (RCC) and 2) dual-functional radar-communication (DFRC) designs. In RCC systems, the radar system and the communication system need to exchange the necessary auxiliary information to perform interference management so as to achieve better collaboration [6], [10], while DFRC systems use fully shared transmitters that transmit the same signal waveform to perform radar and communication functions simultaneously. These two kinds of ISAC systems have both advantages and disadvantages in implementing ISAC functions.

Recently, many researchers have focused on the design of precoding in multiple-input multiple-output (MIMO) ISAC systems, optimizing the transmit precoding matrix through different radar and communication metrics [11]–[22]. MIMO architecture is widely used in ISAC systems to provide waveform diversity for radar target detection [23], precoding gain and spatial multiplexing for multi-user communications. In a MIMO-ISAC system, there is an inherent conflict between the requirements of the radar and the communication components in terms of the antenna placement, the operation region of the power-amplifiers, the signal formats, etc. Typical radar metrics include the signal-to-noise ratio (SNR) of the radar receiver [11], the beampattern mean square error (MSE) [12], the Cramer-Rao bound [13], and the similarity between the designed beamformers and the reference beamformers only for radar systems [14], [15], [17], [18]. At the same time, widely used communication metrics include the achievable rate [19],

[20], the signal-to-interference-plus-noise ratio (SINR) [14], [17], [21] and the multi-user interference (MUI) [12], [15]. Given the system resources, radar performance and communication performance need to be balanced in the waveform design of ISAC system. Therefore, the transmit waveform should be carefully designed to balance the requirements of these two functions and achieve better system performance.

The transmit waveform designs mentioned above [11]–[15], [17]–[22] are all conventional block-level precoding (BLP), i.e., the same precoding matrix is used within a block and the precoding matrix is independent of data symbols. However, since conventional BLP designs usually employ the second-order statistics (e.g., SINR and MSE) as the performance metrics to optimize the average transmit beampattern, the radar sensing performance can be guaranteed only when the number of transmitted symbols is sufficiently large, and not on an instantaneous basis. As a result, the instantaneous transmit beampatterns in different time slots might have significant distortions, which causes severe performance degradation on target detection and parameter estimation if only a limited number of samples are collected. In light of the shortcomings for BLP, symbol-level precoding (SLP) technology has been further adopted in ISAC systems.

Unlike the conventional BLP, SLP is a symbol-dependent approach, which optimizes each instantaneous transmit signal vector based on the specific symbols to be transmitted, rather than simply eliminates MUI at the symbol level [24]–[28]. From the communication perspective, SLP can exploit the symbol information to convert harmful MUI into constructive components, i.e., constructive interference (CI), to reduce the symbol error rate (SER) and perform more reliable multi-user communications. From the radar perspective, the instantaneous transmit beampattern in each time slot can be carefully designed and a well-formed beampattern can be guaranteed with a limited number of waveform samples.

In previous work [29], the transmit vectors for CI-based SLP (CI-SLP) are optimized to minimize the squared error between the obtained and the desired beampattern, subject to CI constraints for communications and power constraints. This work confirms the significant advantage of SLP in enhancing the communication performance over conventional BLP, but the complexity of the optimization problem is difficult to accept due to the non-convex nature of the objective function. In addition, [30] utilizes space-time adaptive processing (STAP) and CI-SLP to implement MIMO ISAC. This scheme shows better performance in the presence of strong signal-dependent clutter. In [31], the authors investigate the SLP-based low-range-sidelobe waveform design for an MIMO-OFDM ISAC system, and the simulation results reveal the performance improvement of radar ranging. All of the above studies take radar performance as the objective function of optimization problems, but the non-convex objective function make the optimization problem difficult to solve directly and the iterative methods are resorted to provide solvable solutions, which require a large number of iterations and make the computational complexity of these schemes difficult to accept. On the other hand, under demanding communication requirements, the probability that these schemes become infeasible will also increase. In other words, the communication performance of these CI-SLP ISAC schemes is limited. In view of these shortcomings, we adopt the symbol-scaling metric in CI-SLP ISAC system and take the communication performance as the objective function of optimization problem, while considering the radar performance as a necessary constraint, which has not been previously investigated in the literature.

Symbol scaling is a competitive CI metric in SLP. Different from the common phase-rotation CI metric [29]–[31] which uses phase relations to perform SLP, the symbol-scaling CI metric decomposes the signal along the decision boundaries and imposes scaling constraints on the decomposed components. The idea of the optimization problem based on symbol scaling is to maximize the minimum scaling factor so as to maximize the exploitation of interference and guarantee the SER performance of the system [32]. Constructing the optimization problem based on symbol scaling can ensure that the objective function is convex, thus reducing the difficulty and computational complexity of solving the problem. In addition, the optimization problem based on symbol scaling can be easily extended from PSK modulation to QAM modulation, which has a wider range of applications [33], [34].

In this paper, we investigate the symbol-scaling based CI-SLP design for MIMO ISAC systems, where a multi-antenna ISAC BS serves multiple single-antenna communication users while simultaneously detecting targets of interest. Specifically, the minimum communication CI scaling factor among the users is maximized under radar performance constraint and power constraint. The main contributions of this paper can be summarized as follows:

1) We initially introduce the symbol-scaling CI metric into the CI-SLP design in ISAC systems. The minimum communication scaling factor among communication users is maximized while satisfying the radar target illumination power requirement and total power budget constraint.
2) In order to solve the proposed ISAC optimization problem, two groups of approximate feasible domains are adopted to transform the optimization problem into convex. In addition, the dual problems of these convex optimization problems are constructed and solved, through which we obtain the corresponding solution of ISAC waveform design and gain meaningful insights for guiding the waveform design. By modifying and adopting Hooke-Jeeves pattern search algorithm, the efficiency of the proposed precoding scheme is highly improved.
3) Furthermore, a weighted symbol-scaling CI-SLP design for ISAC is proposed, which takes the radar performance as a weighted penalty term in the objective function. By analyzing the Lagrangian function and Karush-Kuhn-Tucker (KKT) condition of the weighted optimization, we formulate the corresponding dual problem. It is easy to prove that the dual problem is a simple quadratic programming (QP) problem, and can be easily solved with significantly reduced computational complexity.
4) To be more consistent with the currently used communication systems and achieve better ISAC performance, the CI-SLP ISAC scheme proposed in this paper is further extended from symbol level to block level. The CI-based

BLP (CI-BLP) scheme is more suitable to the currently used communication systems compared with the CI-SLP scheme. In addition, since the CI-BLP scheme can allow a more flexible power allocation in a block level, it can achieve better ISAC performance. The flexible tradeoff between the system performance and complexity can be achieved by modifying the length of each transmission block in CI-BLP.

The simulation results show that the proposed design based on symbol scaling has significant advantages in enhancing the communication performance under the condition that the radar performance satisfy the requirements. In addition, the computational complexity of the proposed schemes can be reduced significantly in comparison with the existing SLP schemes in ISAC systems.

The rest of this paper is organized as follows. Section II introduces the system model, communication model and radar model. The proposed symbol-scaling based CI-SLP design and weighted CI-SLP optimization for ISAC are presented in Sections III and IV, respectively. Section V extends the proposed symbol-scaling based CI-SLP design to the block level. Simulation results are presented in Section VI, and the final conclusions are provided in Section VII.

Notations: Herein, lowercase, boldface lowercase and boldface uppercase letters denote scalars, vectors and matrices, respectively. $\mathbb{R}$ and $\mathbb{C}$ denote the set of real numbers and complex numbers, respectively. Superscripts $^{\mathrm{T}}$ and $^{\mathrm{H}}$ denote the transpose and the transpose-conjugate operations, respectively. The operator $\|\cdot\|_2$ denotes the 2-norm of a vector. $\Re\{\cdot\}$ and $\Im\{\cdot\}$ extract the real and imaginary parts of the argument, respectively. We define $\mathbf{I}_N$ as the $N \times N$ identity matrix, and $\mathbf{O}_N$ as the $N \times N$ all-zero matrix. Finally, $\mathbf{1}$ and $\mathbf{0}$ denote all-one vector and all-zero vector, respectively.

II. System Model and Preliminaries

A. System Model

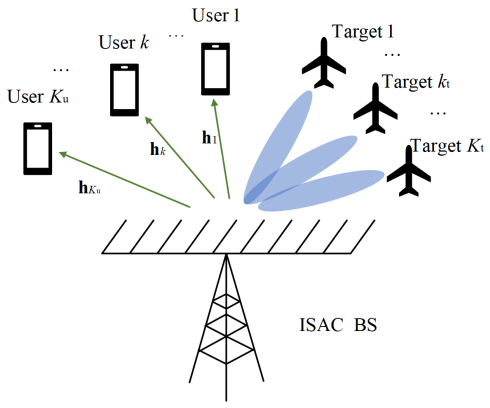

Fig. 1. The ISAC system with one multi-antenna ISAC BS serving multiple communication users while sensing targets of interest.

We consider a MIMO ISAC system as shown in Fig.1, where the multi-antenna ISAC BS simultaneously transmits radar probing waveforms to the targets and communication symbols to the downlink users. The ISAC BS is equipped with a uniform linear array (ULA) of N antennas, serving K_{u} single-antenna users while detecting K_{t} targets at the same time, generally with $K_{\mathrm{u}} \leq N$ and $K_{\mathrm{t}} \leq N$. The same antenna array is used for both transmitting and receiving in different time slots via time-division (TD) protocol.

In this paper, the transmit signal matrix $\mathbf{X} = [\mathbf{x}[1], \mathbf{x}[2], \cdots, \mathbf{x}[L]] \in \mathbb{C}^{N\times L}$ is used as the baseband representation of the ISAC waveform for both radar and communication operations, where $\mathbf{x}[l] = [x_1[l], x_2[l], \cdots, x_N[l]]^{\mathrm{T}} \in \mathbb{C}^{N\times 1}$ is the corresponding ISAC waveform in the l-slot with $l \in \{1, 2, \cdots, L\}$. In addition, the data symbol vector for K_{u} users in the l-th slot is denoted by $\mathbf{s}[l] = [s_1[l], s_2[l], \cdots, s_{K_{\mathrm{u}}}[l]]^{\mathrm{T}} \in \mathbb{C}^{K_{\mathrm{u}}\times 1}$, which is assumed to be drawn from a unit-norm PSK constellation. Unlike conventional BLP designs, SLP in general employs a mapping from $\mathbf{s}[l]$ to $\mathbf{x}[l]$, and optimizes $\mathbf{x}[l]$ directly according to the instantaneous symbol vector $\mathbf{s}[l]$ instead of using second-order statistics-based metrics.

B. Communication Model

The received signal for the k-th user in the l-th time slot is

$$y_k[l] = \mathbf{h}_k^{\mathrm{T}}\mathbf{x}[l] + z_k^{\mathrm{c}}[l], \tag{1}$$

where $\mathbf{h}_k \in \mathbb{C}^{N\times 1}$ is the channel between the ISAC BS and user k, and $z_k^{\mathrm{c}}[l] \sim \mathcal{CN}(0, \sigma_{\mathrm{c}}^2)$ is the additive noise of user k in the l-th slot with σ_{c}^2 being the noise power.

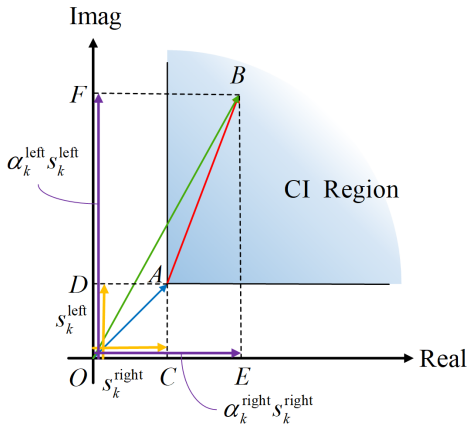

Fig. 2. Geometric diagram of the symbol-scaling CI metric for QPSK.

To illustrate the symbol-scaling CI meric introduced in [28], we depict one quarter of a QPSK constellation in Fig. 2 as an example, where we drop the time slot index $[l]$ for conciseness. Without loss of generality, we assume that $\overrightarrow{OA}$ is the nominal constellation point for user $k \in \{1, 2, \cdots, K\}$ in slot l, i.e.,

$$\overrightarrow{OA} = s_k[l]. \tag{2}$$

$\overrightarrow{OB}$ represents the noiseless received signal with interference, which can be expressed as

$$\overrightarrow{OB} = \overrightarrow{OA} + \overrightarrow{AB} = \mathbf{h}_k^{\mathrm{T}}\mathbf{x}[l], \tag{3}$$

based on the geometry, and $\overrightarrow{AB}$ can be regarded as the sum CI from other user streams.

Different from the common phase-rotation CI metric which uses phase relations for SLP [29]–[31], we try to leverage the the symbol-scaling CI metric for SLP, which decomposes the signal along the decision boundaries and imposes scaling constraints on the decomposed components. One of the advantages for the symbol-scaling based SLP method is that the precoding optimization problem based on symbol scaling can be easily extended to QAM modulation [33]. Hence, we leverage the symbol-scaling metric to design the SLP scheme for enhancing the system ISAC performance.

Based on the symbol-scaling metric, $\overrightarrow{OA}$ is decomposed along the two decision boundaries of the QPSK modulation to obtain $\overrightarrow{OC}$ and $\overrightarrow{OD}$:

$$\begin{aligned}\overrightarrow{OA} &= \overrightarrow{OC} + \overrightarrow{OD} \\ &= s_k^{\text{right}}[l] + s_k^{\text{left}}[l]. \end{aligned} \tag{4}$$

Following a similar procedure, the noiseless received signal $\overrightarrow{OB}$ can also be decomposed along the two decision boundaries as

$$\begin{aligned}\overrightarrow{OB} &= \overrightarrow{OE} + \overrightarrow{OF} \\ &= \alpha_k^{\text{right}}[l]\, s_k^{\text{right}}[l] + \alpha_k^{\text{left}}[l]\, s_k^{\text{left}}[l], \end{aligned} \tag{5}$$

where $\alpha_k^{\text{right}}[l]$ and $\alpha_k^{\text{left}}[l]$ are non-negative scaling factors. We can observe that the value of α_k^{right} or α_k^{left} represents the effect of inter-user CI, and a larger value of α_k^{right} or α_k^{left} means that the symbol can be pushed further away from one of its decision boundary as shown in Fig. 2.

By following the transformations in [32], we can construct a coefficient matrix $\mathbf{M} \in \mathbb{R}^{2K_{\text{u}} \times 2N}$ and obtain:

$$\boldsymbol{\alpha}_{\text{E}} = \mathbf{M}\mathbf{x}_{\text{E}}, \tag{6}$$

where $\boldsymbol{\alpha}_{\text{E}} \in \mathbb{R}^{2K_{\text{u}} \times 1}$ and $\mathbf{x}_{\text{E}} \in \mathbb{R}^{2N \times 1}$ are defined as

$$\begin{aligned}\boldsymbol{\alpha}_{\text{E}} &= \left[\alpha_1^{\text{right}}[l], \cdots, \alpha_{K_{\text{u}}}^{\text{right}}[l], \alpha_1^{\text{left}}[l], \cdots, \alpha_{K_{\text{u}}}^{\text{left}}[l]\right]^{\text{T}}, \\ \mathbf{x}_{\text{E}} &= \left[\Re(\mathbf{x}[l])^{\text{T}}, \Im(\mathbf{x}[l])^{\text{T}}\right]^{\text{T}}. \end{aligned} \tag{7}$$

The construction of $\mathbf{M}$ is shown in Appendix A, which directly follows Section IV-A of [32].

C. Radar Model

For the radar sensing, the incident signal at the k_{t}-th target location is expressed as

$$r_{k_{\text{t}}}[l] = \beta_{k_{\text{t}}} \mathbf{a}(\theta_{k_{\text{t}}})^{\text{H}} \mathbf{x}[l], \tag{8}$$

where $\mathbf{a}(\theta_{k_{\text{t}}}) = \left[1, e^{j\sin\theta_{k_{\text{t}}}}, \cdots, e^{j(N-1)\sin\theta_{k_{\text{t}}}}\right]^{\text{T}} \in \mathbb{C}^{N\times 1}$ is the steering vector of the BS towards the target with $\theta_{k_{\text{t}}}$ as the corresponding azimuth angle. $\beta_{k_{\text{t}}}$ accounts for the effective channel propagation coefficient. Thus, the illumination power [35], [36] towards the k_{t}-th target is given by

$$\begin{aligned}P_{k_{\text{t}}} &= \beta_{k_{\text{t}}}^2 \cdot \left|\mathbf{a}(\theta_{k_{\text{t}}})^{\text{H}} \mathbf{x}[l]\right|^2 \\ &= \beta_{k_{\text{t}}}^2 \left(\left|\mathbf{a}_{\text{E},k_{\text{t}}}^{\text{T}} \mathbf{x}_{\text{E}}\right|^2 + \left|\mathbf{b}_{\text{E},k_{\text{t}}}^{\text{T}} \mathbf{x}_{\text{E}}\right|^2\right), \end{aligned} \tag{9}$$

where $\mathbf{a}_{\text{E},k_{\text{t}}} \in \mathbb{C}^{2N\times 1}$ and $\mathbf{b}_{\text{E},k_{\text{t}}} \in \mathbb{C}^{2N\times 1}$ are defined as

$$\begin{aligned}\mathbf{a}_{\text{E},k_{\text{t}}} &= \left[\Re(\mathbf{a}(\theta_{k_{\text{t}}}))^{\text{T}}, \Im(\mathbf{a}(\theta_{k_{\text{t}}}))^{\text{T}}\right]^{\text{T}}, \\ \mathbf{b}_{\text{E},k_{\text{t}}} &= \left[-\Im(\mathbf{a}(\theta_{k_{\text{t}}}))^{\text{T}}, \Re(\mathbf{a}(\theta_{k_{\text{t}}}))^{\text{T}}\right]^{\text{T}}. \end{aligned} \tag{10}$$

The radar illumination power is expected to be no less than a preset minimum to guarantee the detection probabilities. Hence the radar constraint is formulated as

$$\beta_{k_{\text{t}}}^2 \left(\left|\mathbf{a}_{\text{E},k_{\text{t}}}^{\text{T}} \mathbf{x}_{\text{E}}\right|^2 + \left|\mathbf{b}_{\text{E},k_{\text{t}}}^{\text{T}} \mathbf{x}_{\text{E}}\right|^2\right) \geq p_{\text{r},k_{\text{t}}}, \tag{11}$$

where $p_{\text{r},k_{\text{t}}} = \sigma_{\text{r}}^2 \Gamma_{\text{r}}$ is the preset minimum illumination power requirement for the k_{t}-th target. Here, σ_{r}^2 and Γ_{r} represent the radar noise power and the preset radar threshold.

III. Symbol-Scaling CI-SLP Design for ISAC

A. Problem Formulation

Based on the above description, in this paper, we aim to design the transmit signal vector $\mathbf{x}_{\text{E}}$ to maximize the minimum entry in $\boldsymbol{\alpha}_{\text{E}}$, which can make the received signal of each user far away from the decision boundary on both sides, thus improving the overall communication SER performance during the considered time period. As for the radar sensing performance, we introduce the illumination power requirement for the k_{t}-th target. Therefore, the CI-SLP ISAC optimization problem for single target detection is formulated as

$$\mathcal{P}_0: \max_{\mathbf{x}_{\text{E}}} \min_{i} \alpha_i \tag{12}$$

$$\text{s.t.} \quad \boldsymbol{\alpha}_{\text{E}} = \mathbf{M}\mathbf{x}_{\text{E}}, \tag{12a}$$

$$\beta_{k_{\text{t}}}^2 \left(\left|\mathbf{a}_{\text{E},k_{\text{t}}}^{\text{T}} \mathbf{x}_{\text{E}}\right|^2 + \left|\mathbf{b}_{\text{E},k_{\text{t}}}^{\text{T}} \mathbf{x}_{\text{E}}\right|^2\right) \geq p_{\text{r},k_{\text{t}}}, \tag{12b}$$

$$\|\mathbf{x}_{\text{E}}\|_2^2 \leq p_0, \tag{12c}$$

where α_i represents the i-th entry in $\boldsymbol{\alpha}_{\text{E}}$, and p_0 represents the transmit power budget per symbol slot.

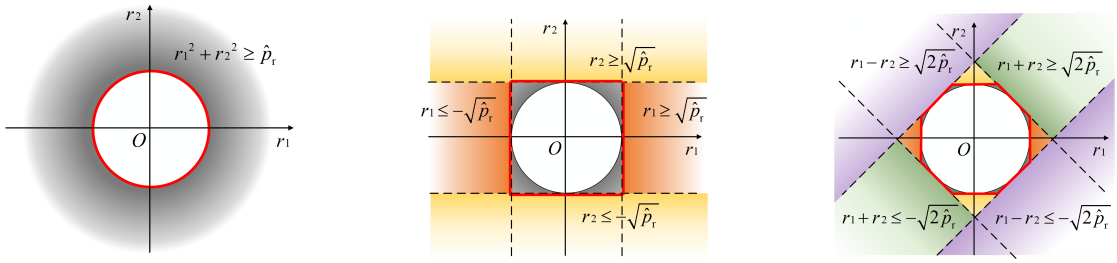

Fig. 3. (a) The constraint on the target illumination power. (b) The first group of feasible domains. (c) The second group of feasible domains.

We note that the total power constraint (12c) can be extended to other power-related constraints, such as the following per-antenna power constraint

$$|x_{\mathrm{E},n}|^2 + |x_{\mathrm{E},n+N}|^2 \leq \frac{p_0}{N},\ \forall n \in \{1, \cdots, N\}, \tag{13}$$

which is also a convex constraint. Here, $x_{\mathrm{E},n}$ represents the n-th entry in $\mathbf{x}_{\mathrm{E}}$.

Note that $\mathcal{P}_0$ is non-convex because the constraint on the target illumination power (12b) is non-convex. Therefore, we first deal with the constraint of the target illumination power.

B. Problem Transformation

By defining $\hat{p}_{\mathrm{r}} = \frac{p_{\mathrm{r},k_{\mathrm{t}}}}{\beta^2_{k_{\mathrm{t}}}}$, $r_1 = \mathbf{a}^{\mathrm{T}}_{\mathrm{E},k_{\mathrm{t}}}\mathbf{x}_{\mathrm{E}}$ and $r_2 = \mathbf{b}^{\mathrm{T}}_{\mathrm{E},k_{\mathrm{t}}}\mathbf{x}_{\mathrm{E}}$, the constraint on the target illumination power constraint (12b) can be written as:

$$r_1^2 + r_2^2 \geq \hat{p}_{\mathrm{r}}. \tag{14}$$

This constraint indicates that the feasible solutions of r_1 and r_2 fall outside a circle shown in Fig. 3(a), which is a non-convex constraint. We try to utilize several tangent lines of the circle as its approximations, so as to transform the non-convex constraint into convex. As shown in Fig. 3(b) and 3(c), we select two groups of approximate feasible domains, and the details of the domains are given below:

1) The first group has four tangent lines, and the approximated feasible region includes four convex sets which is given below

$$\begin{aligned}
&\mathbb{S}_1 = \mathbb{T}_1 \cup \mathbb{T}_2,\\
&\mathbb{T}_1 = \left\{\mathbf{x}_{\mathrm{E}} | r_1 \leq -\sqrt{\hat{p}_{\mathrm{r}}}\right\} \cup \left\{\mathbf{x}_{\mathrm{E}} | r_1 \geq \sqrt{\hat{p}_{\mathrm{r}}}\right\},\\
&\mathbb{T}_2 = \left\{\mathbf{x}_{\mathrm{E}} | r_2 \leq -\sqrt{\hat{p}_{\mathrm{r}}}\right\} \cup \left\{\mathbf{x}_{\mathrm{E}} | r_2 \geq \sqrt{\hat{p}_{\mathrm{r}}}\right\}.
\end{aligned} \tag{15}$$

2) The second group has eight tangent lines, and the approximated feasible region includes eight convex sets which is given below

$$\begin{aligned}
&\mathbb{S}_2 = \mathbb{S}_1 \cup \mathbb{T}_3 \cup \mathbb{T}_4,\\
&\mathbb{T}_3 = \left\{\mathbf{x}_{\mathrm{E}} | r_1 + r_2 \leq -\sqrt{2\hat{p}_{\mathrm{r}}}\right\} \cup \left\{\mathbf{x}_{\mathrm{E}} | r_1 + r_2 \geq \sqrt{2\hat{p}_{\mathrm{r}}}\right\},\\
&\mathbb{T}_4 = \left\{\mathbf{x}_{\mathrm{E}} | r_1 - r_2 \leq -\sqrt{2\hat{p}_{\mathrm{r}}}\right\} \cup \left\{\mathbf{x}_{\mathrm{E}} | r_1 - r_2 \geq \sqrt{2\hat{p}_{\mathrm{r}}}\right\}.
\end{aligned} \tag{16}$$

Through the above approximation, the original optimization problem $\mathcal{P}_0$ can be transformed into the following problem $\mathcal{P}_1$:

$$\begin{aligned}
\mathcal{P}_1:\ &\max_{\mathbf{x}_{\mathrm{E}}}\ \min_{i}\ \alpha_i && (17)\\
&\text{s.t.}\ \ \boldsymbol{\alpha}_{\mathrm{E}} = \mathbf{M}\mathbf{x}_{\mathrm{E}}, && (17a)\\
&\qquad \mathbf{x}_{\mathrm{E}} \in \mathbb{S}_n, && (17b)\\
&\qquad \|\mathbf{x}_{\mathrm{E}}\|_2^2 \leq p_0, && (17c)
\end{aligned}$$

where $n \in \{1, 2\}$. Although $\mathbb{S}_1$ (or $\mathbb{S}_2$) is still not convex and we cannot solve this non-convex optimization problem directly, it is easy to note that the above two groups of feasible domains $\mathbb{S}_1$ and $\mathbb{S}_2$ are all unions of some simple convex sets. Therefore, the solution of the approximated optimization problem $\mathcal{P}_1$ can be easily transformed into solving several convex optimization subproblems each with a convex sub-set. Note that the approximated problem $\mathcal{P}_1$ with the second group of feasible domains $\mathbb{S}_2$ has smaller gap with the original problem $\mathcal{P}_0$, but the corresponding complexity is higher compared with the first group $\mathbb{S}_1$, which will be confirmed in Section VI. Through choosing different groups can achieve different trade-offs between the ISAC performance and computational complexity.

Remark 1: *It is true that we can further increase the number of tangent lines to get more accurate approximation but at the sacrifice of higher complexity. When the number of tangent lines increases to $2M$, the approximated feasible region will include $2M$ convex sets which is given as $\mathbb{S}$.*

$$\begin{aligned}
&\mathbb{S} = \mathbb{T}_1 \cup \cdots \cup \mathbb{T}_M,\\
&\mathbb{T}_m = \left\{\mathbf{x}_{\mathrm{E}} | \frac{\cos\phi_m}{\sin\phi_m} r_1 + r_2 \leq -\sqrt{\hat{p}_{\mathrm{r}}}\left(\sin\phi_m + \frac{\cos^2\phi_m}{\sin\phi_m}\right)\right\}\\
&\qquad \cup \left\{\mathbf{x}_{\mathrm{E}} | \frac{\cos\phi_m}{\sin\phi_m} r_1 + r_2 \geq \sqrt{\hat{p}_{\mathrm{r}}}\left(\sin\phi_m + \frac{\cos^2\phi_m}{\sin\phi_m}\right)\right\},\\
&\phi_m = \frac{\pi}{M}(m-1),\ \forall m \in \{1, \cdots, M\}.
\end{aligned} \tag{18}$$

Specifically, the convex optimization subproblems of the approximated optimization problem $\mathcal{P}_1$, corresponding to different simple convex sets, can be written in a unified form:

$$\begin{aligned}
\mathcal{P}_2:\ &\max_{\mathbf{x}_{\mathrm{E}}}\ \min_{i}\ \alpha_i && (19)\\
&\text{s.t.}\ \ \boldsymbol{\alpha}_{\mathrm{E}} = \mathbf{M}\mathbf{x}_{\mathrm{E}}, && (19a)\\
&\qquad \mathbf{c}^{\mathrm{T}}\mathbf{x}_{\mathrm{E}} \geq d, && (19b)\\
&\qquad \|\mathbf{x}_{\mathrm{E}}\|_2^2 \leq p_0, && (19c)
\end{aligned}$$

where $\mathbf{c}$ and d in (19b) take different values according to different convex sets, which are listed in Appendix B.

Further, we can equivalently transform problem $\mathcal{P}_2$ to the following minimization problem $\mathcal{P}_3$ by introducing an auxiliary variable t

$$\begin{aligned}
\mathcal{P}_3:\ &\min_{t,\mathbf{x}_{\mathrm{E}}}\ -t && (20)\\
&\text{s.t.}\ \ \mathbf{M}\mathbf{x}_{\mathrm{E}} \geq t \cdot \mathbf{1}, && (20a)\\
&\qquad \mathbf{c}^{\mathrm{T}}\mathbf{x}_{\mathrm{E}} \geq d, && (20b)\\
&\qquad \|\mathbf{x}_{\mathrm{E}}\|_2^2 \leq p_0. && (20c)
\end{aligned}$$

It is easy to prove that $\mathcal{P}_3$ is a standard convex optimization problem that can be directly solved via existing convex optimization tools such as CVX [37].

Therefore, for each group of feasible domains, we just need to solve the optimization subproblems $\mathcal{P}_3$ with specific $\mathbf{c}$ and d to get sets of local optimal solutions to the approximated optimization problem $\mathcal{P}_1$, and then we choose the solution with the best result among these local optimal solutions as the global optimal solution. In particular, assuming that the number of $\mathcal{P}_3$ to be solved is N_{p}, then N_{p} local optimal solutions will be obtained. For example, $N_{\mathrm{p}} = 4$ and 8 for the first and second group of feasible domains, respectively. By denoting these N_{p} local optimal solutions as $\left\{\left(t_1^*, \mathbf{x}_{\mathrm{E},1}^*\right), \cdots, \left(t_{N_{\mathrm{p}}}^*, \mathbf{x}_{\mathrm{E},N_{\mathrm{p}}}^*\right)\right\}$, then the global optimal solution $\mathbf{x}_{\mathrm{E}}^* = \mathbf{x}_{\mathrm{E},n}^*$ can be determined

as follows:

$$n = \underset{i=\{1,\cdots,N_{\mathrm{p}}\}}{\operatorname{argmax}} \; t_i^*. \tag{21}$$

Depending on the chosen group of feasible domains, N_{p} optimization subproblems $\mathcal{P}_3$ needs to be solved. The computational complexity of $\mathcal{P}_3$ determines the overall design complexity, which can be further reduced by proposing an efficient solving method. Therfore, a more efficient algorithm is developed in the following subsection, which solves the dual problem of $\mathcal{P}_3$ with the aid of the modified Hook-Jeeves Pattern Search algorithm [38].

Remark 2: *The optimization problem $\mathcal{P}_0$ can be extended to the case of multiple targets by introducing multi-target radar constraints, i.e., increasing the number of radar illumination power constraints. The CI-SLP ISAC optimization problem for multiple target detection can be transformed into several convex optimization problems, similar to the case of single target detection. The simulation results of multiple target detection will be presented in Section V.*

C. An Efficient Lagrangian Algorithm to solve $\mathcal{P}_3$

Fortunately, it is further noted through numerical results that the obtained $\mathbf{x}_{\mathrm{E}}$ from the problem $\mathcal{P}_3$ mostly meet the strict-equality radar requirement, i.e. the optimization problem $\mathcal{P}_3$ can be further approximated as $\mathcal{P}_4$, given by

$$\begin{aligned} \mathcal{P}_4: \; \min_{t,\mathbf{x}_{\mathrm{E}}} \; & -t && (22)\\ \text{s.t.} \; & \mathbf{M}\mathbf{x}_{\mathrm{E}} \geq t\cdot\mathbf{1}, && (22a)\\ & \mathbf{c}^{\mathrm{T}}\mathbf{x}_{\mathrm{E}} = d, && (22b)\\ & \|\mathbf{x}_{\mathrm{E}}\|_2^2 \leq p_0. && (22c) \end{aligned}$$

In order to further evaluate the deviation of the problem $\mathcal{P}_4$ from the problem $\mathcal{P}_3$, we do a number of random simulations to check the results numerically. We define η as the ratio that $\mathbf{x}_{\mathrm{E}}$ obtained from problem $\mathcal{P}_3$ does not satisfy the radar equality constraint, and this ratio can represent the deviation of the problem $\mathcal{P}_4$ from the problem $\mathcal{P}_3$. We have $0 \leq \eta \leq 1$, and the deviation between problem $\mathcal{P}_4$ and problem $\mathcal{P}_3$ can be ignored if $\eta = 0$, which means that the equivalence approximately holds. To study this numerically and check the conditions, we present the value of η with respect to the required radar threshold $\Gamma_{\mathrm{r}} = \frac{p_{\mathrm{r},k_{\mathrm{t}}}}{\sigma_{\mathrm{r}}^2}$ in Table I, where we have assumed that the number of transmit antennas is $N = 10$, the number of users is $K_{\mathrm{u}} = 3$, and the radar noise power is $\sigma_{\mathrm{r}}^2 = 20$dBm. Hence, the larger the value of Γ_{r}, the more stringent radar performance is required according to radar constraint (11). The total number of experiments is 1000, and we list the simulation results in the following table.

TABLE I
η with respect to the radar threshold Γ_{r}, $N = 10$, $K_{\mathrm{u}} = 3$, $\sigma_{\mathrm{r}}^2 = 20$dBm.

Γ_{r}	15dB	16dB	17dB	18dB	19dB
η	0.020	0.007	0.003	0	0

It is observed that the ratio η is quite small and it decreases with the increase in the radar threshold Γ_{r}, which means that the solution obtained via the problem $\mathcal{P}_3$ mostly meets the strict-equality radar requirement in the considered ISAC system especially with a larger radar threshold Γ_{r}.

We can solve $\mathcal{P}_4$ optimally by solving its dual problem, because the Slaters condition is satisfied for the convex optimization problem $\mathcal{P}_4$ [37]. The Lagrangian dual function of $\mathcal{P}_4$ is given by

$$\begin{aligned} \mathcal{L}\left(\mathbf{x}_{\mathrm{E}}, t, \boldsymbol{\lambda}, \mu, \nu\right) = & -t + \boldsymbol{\lambda}^{\mathrm{T}}\left(t\cdot\mathbf{1} - \mathbf{M}\mathbf{x}_{\mathrm{E}}\right) \\ & + \mu\left(\|\mathbf{x}_{\mathrm{E}}\|_2^2 - p_0\right) + \nu\left(d - \mathbf{c}^{\mathrm{T}}\mathbf{x}_{\mathrm{E}}\right), \end{aligned} \tag{23}$$

where $\boldsymbol{\lambda}$, μ and ν are the dual variables associated with the inequality constraints (22a), (22c) and the equality constraint (22b) respectively. Accordingly, the KKT conditions for the optimality of problem $\mathcal{P}_4$ can be formulated as

$$\frac{\partial\mathcal{L}}{\partial t} = \mathbf{1}^{\mathrm{T}}\boldsymbol{\lambda} - 1 = 0, \tag{24a}$$

$$\frac{\partial\mathcal{L}}{\partial\mathbf{x}_{\mathrm{E}}} = -\mathbf{M}^{\mathrm{T}}\boldsymbol{\lambda} + 2\mu\mathbf{x}_{\mathrm{E}} - \nu\mathbf{c} = \mathbf{0}, \tag{24b}$$

$$\boldsymbol{\lambda}^{\mathrm{T}}\left(t\cdot\mathbf{1} - \mathbf{M}\mathbf{x}_{\mathrm{E}}\right) = 0, \;\; \lambda_k \geq 0, \;\; \forall 1 \leq k \leq 2K_{\mathrm{u}}, \tag{24c}$$

$$\mu\left(\|\mathbf{x}_{\mathrm{E}}\|_2^2 - p_0\right) = 0, \;\; \mu \geq 0. \tag{24d}$$

Based on the KKT conditions, we can obtain $\mu > 0$, which will be proved in Appendix C. This means that the total power constraint is active when the optimality is achieved, i.e.,

$$\|\mathbf{x}_{\mathrm{E}}\|_2^2 = p_0. \tag{25}$$

Considering $\mu > 0$, based on (24b), we can obtain an expression for the optimal transmit signal vector $\mathbf{x}_{\mathrm{E}}$ as a function of the Lagrange multipliers in a closed form:

$$\mathbf{x}_{\mathrm{E}} = \frac{1}{2\mu}\left(\mathbf{M}^{\mathrm{T}}\boldsymbol{\lambda} + \nu\mathbf{c}\right). \tag{26}$$

By substituting (26) into (25) and (22b) respectively, and after some simple mathematical processing, we can obtain the expressions of μ and ν:

$$\mu = \sqrt{\frac{\mathbf{c}^{\mathrm{T}}\mathbf{c}\cdot\boldsymbol{\lambda}^{\mathrm{T}}\mathbf{M}\mathbf{M}^{\mathrm{T}}\boldsymbol{\lambda} - \left(\mathbf{c}^{\mathrm{T}}\mathbf{M}^{\mathrm{T}}\boldsymbol{\lambda}\right)^2}{4p_0\mathbf{c}^{\mathrm{T}}\mathbf{c} - 4d}}, \tag{27}$$

$$\nu = \frac{1}{\mathbf{c}^{\mathrm{T}}\mathbf{c}}\left(2\mu d - \mathbf{c}^{\mathrm{T}}\mathbf{M}^{\mathrm{T}}\boldsymbol{\lambda}\right). \tag{28}$$

Next, by substituting (24a), (24d), (22b) and (26) into (23), we can transform the objective function of the dual problem into a function of lambda, indicated as $\mathcal{F}\left(\boldsymbol{\lambda}\right)$. Hence, the dual problem of $\mathcal{P}_4$ can be formulated as problem $\mathcal{P}_5$, shown at the top of the next page.

It can be observed that the objective function of optimization problem $\mathcal{P}_5$ is non-convex and quite complex, thus problem $\mathcal{P}_5$ is difficult to be solved directly. However, the constraints of $\mathcal{P}_5$ are very simple, and this feature implies that the search algorithm can be considered. We adopt the Hooke-Jeeves pattern search method [38] to efficiently solve $\mathcal{P}_5$ via an iterative manner to obtain the optimal solution. This iterative method consists of two steps: One step is to detect the most advantageous descent direction by moving the basepoint along all dimensions in turn with a certain step size; The other step is to update the variable along this direction with a certain

$$\mathcal{P}_5: \min_{\boldsymbol{\lambda}} \ \mathcal{F}(\boldsymbol{\lambda}) = \frac{\sqrt{p_0\mathbf{c}^{\mathrm{T}}\mathbf{c}-d}}{\mathbf{c}^{\mathrm{T}}\mathbf{c}} \cdot \sqrt{\mathbf{c}^{\mathrm{T}}\mathbf{c}\boldsymbol{\lambda}^{\mathrm{T}}\mathbf{M}\mathbf{M}^{\mathrm{T}}\boldsymbol{\lambda} - (\mathbf{c}^{\mathrm{T}}\mathbf{M}^{\mathrm{T}}\boldsymbol{\lambda})^2} + \frac{\sqrt{d}}{\mathbf{c}^{\mathrm{T}}\mathbf{c}} \cdot \mathbf{c}^{\mathrm{T}}\mathbf{M}^{\mathrm{T}}\boldsymbol{\lambda}$$
$$\text{s.t.} \ \ \mathbf{1}^{\mathrm{T}}\boldsymbol{\lambda} = 1,$$
$$\lambda_i \geq 0, \ \forall i \in \{1, \cdots, 2K_{\mathrm{u}}\}. \tag{29}$$

step size until the performance cannot be improved, and then the step size will be reduced to half of this value for the next iteration, and the process is repeated until a convergence criterion is met. Because of the additional constraint $\mathbf{1}^{\mathrm{T}}\boldsymbol{\lambda} = 1$, the traditional Hooke-Jeeves pattern search algorithm cannot be used directly, and thus we proposed a modified Hooke-Jeeves pattern search algorithm, which is summarized in Algorithm 1.

Algorithm 1 The Modified Hooke-Jeeves Pattern Search Algorithm

Input: $\mathbf{M}$, p_0, $\mathbf{c}$, d, $N_{\max}$, d_{th}, $\mathbf{u}_1, \mathbf{u}_2, \cdots, \mathbf{u}_{2K_{\mathrm{u}}}$
Initial $\boldsymbol{\lambda}_x^1 = \boldsymbol{\lambda}_y^1$, $d = 1$, $iter = 1$;
while $iter \leq N_{\max}$ and $d \geq d_{\mathrm{th}}$ **do**
  for $i = 1 : 2K_{\mathrm{u}}$ **do**
    $\boldsymbol{\lambda}_a = \boldsymbol{\lambda}_y^i + d\mathbf{u}_i, \boldsymbol{\lambda}_a = \boldsymbol{\lambda}_a / \left(\mathbf{1}^{\mathrm{T}}\boldsymbol{\lambda}_a\right)$;
    if $\mathcal{F}(\boldsymbol{\lambda}_a) < \mathcal{F}\left(\boldsymbol{\lambda}_y^i\right)$ **then**
      $\boldsymbol{\lambda}_y^{i+1} = \max\left\{\mathbf{0}, \boldsymbol{\lambda}_y^i + d\mathbf{u}_i\right\}$;
      $\boldsymbol{\lambda}_y^{i+1} = \boldsymbol{\lambda}_y^{i+1} / \left(\mathbf{1}^{\mathrm{T}}\boldsymbol{\lambda}_y^{i+1}\right)$, go back to 5;
    end if
    $\boldsymbol{\lambda}_b = \boldsymbol{\lambda}_y^i - d\mathbf{u}_i, \boldsymbol{\lambda}_b = \boldsymbol{\lambda}_b / \left(\mathbf{1}^{\mathrm{T}}\boldsymbol{\lambda}_b\right)$;
    if $\mathcal{F}(\boldsymbol{\lambda}_b) < \mathcal{F}\left(\boldsymbol{\lambda}_y^i\right)$ **then**
      $\boldsymbol{\lambda}_y^{i+1} = \max\left\{\mathbf{0}, \boldsymbol{\lambda}_y^i - d\mathbf{u}_i\right\}$;
      $\boldsymbol{\lambda}_y^{i+1} = \boldsymbol{\lambda}_y^{i+1} / \left(\mathbf{1}^{\mathrm{T}}\boldsymbol{\lambda}_y^{i+1}\right)$, go back to 5;
    end if
  end for
  if $\mathcal{F}\left(\boldsymbol{\lambda}_y^{2K_{\mathrm{u}}+1}\right) \geq \mathcal{F}\left(\boldsymbol{\lambda}_x^{iter}\right)$ **then**
    Go to 24;
  else
    $\boldsymbol{\lambda}_x^{iter+1} = \boldsymbol{\lambda}_y^{2K_{\mathrm{u}}+1}$;
    $\boldsymbol{\lambda}_y^1 = \max\left\{\mathbf{0}, \boldsymbol{\lambda}_x^{iter+1} + d\left(\boldsymbol{\lambda}_x^{iter+1} - \boldsymbol{\lambda}_x^{iter}\right)\right\}$;
    $iter = iter + 1$, go back to 5;
  end if
  if $d > d_{\mathrm{th}}$ **then**
    $d = d/2, \boldsymbol{\lambda}_y^1 = \boldsymbol{\lambda}_x^{iter}, \boldsymbol{\lambda}_x^{iter+1} = \boldsymbol{\lambda}_x^{iter}$
    $iter = iter + 1$, go back to 5;
  end if
end while
$\boldsymbol{\lambda}^* = \boldsymbol{\lambda}_x^{iter}$.
Output: $\boldsymbol{\lambda}^*$

In Algorithm 1, we use $N_{\max}$ to denote the maximum number of iterations, d_{th} indicates the convergence threshold, and $\mathbf{u}_1, \mathbf{u}_2, \cdots, \mathbf{u}_{2K_{\mathrm{u}}}$ are the unit vectors on each dimension of $\boldsymbol{\lambda}$. After obtaining $\boldsymbol{\lambda}^*$ of the dual problem, the optimal $\mathbf{x}_{\mathrm{E}}$ can be calculated using the results in (26), (27) and (28). Furthermore, the corresponding optimal objective value t^* can be obtained as:

$$t^* = \min\left(\mathbf{M}\mathbf{x}_{\mathrm{E}}^*\right). \tag{30}$$

Finally, the optimal transmit signal vector in the l-slot can be obtained:

$$\mathbf{x}[l] = \begin{bmatrix}\mathbf{I}_N & \mathbf{O}_N\end{bmatrix} \cdot \mathbf{x}_{\mathrm{E}}^* + j \cdot \begin{bmatrix}\mathbf{O}_N & \mathbf{I}_N\end{bmatrix} \cdot \mathbf{x}_{\mathrm{E}}^*, \tag{31}$$

based on the definition of $\mathbf{x}_{\mathrm{E}}$ in (7). The proposed symbol-scaling CI-SLP design for ISAC in this section can be summarized by the following Algorithm 2.

Algorithm 2 Symbol-Scaling CI-SLP Design for ISAC

Input: $\mathbf{s}_k[l]$, $\mathbf{H} = [\mathbf{h}_1, \cdots, \mathbf{h}_{K_{\mathrm{u}}}]^{\mathrm{T}}$, $\mathbf{a}(\theta)$, p_0, $\hat{p}_{\mathrm{r}}$
Initial $\mathbf{M}$, $\mathbf{a}_{\mathrm{E}}$ and $\mathbf{b}_{\mathrm{E}}$;
Solve N_{p} optimization problems $\mathcal{P}_5$ by Algorithm 1, with specific $\mathbf{c}$ and d according to the composition of the feasible domain and obtain $\left\{\boldsymbol{\lambda}_1^*, \cdots, \boldsymbol{\lambda}_{N_{\mathrm{p}}}^*\right\}$;
Compute $\left\{\left\{\mu_1^*, \nu_1^*, \mathbf{x}_{\mathrm{E},1}^*, t_1^*\right\}, \cdots, \left\{\mu_{N_{\mathrm{p}}}^*, \nu_{N_{\mathrm{p}}}^*, \mathbf{x}_{\mathrm{E},N_{\mathrm{p}}}^*, t_{N_{\mathrm{p}}}^*\right\}\right\}$ by (27), (28), (26) and (30);
Find the global optimal solution $\mathbf{x}_{\mathrm{E}}^*$ by (21);
Obtain the transmit signal vector $\mathbf{x}[l]$ by (31).
Output: $\mathbf{x}[l]$

D. Complexity Analysis

The computational complexity for the methods proposed in Section III-B and III-C mainly comes from solving problem $\mathcal{P}_3$ and $\mathcal{P}_5$.

Firstly, we analyze the computational complexity of problem $\mathcal{P}_3$ with CVX. Since problem $\mathcal{P}_3$ is a convex optimization problem and involves only linear matrix inequality (LMI) and second-order cone (SOC) constraints, it can be solved by a standard interior-point method (IPM) embedded in CVX. The complexity of a generic IPM consists of two parts: (1) iteration complexity and (2) per-iteration computation cost [39]. Considering problem $\mathcal{P}_3$, which has $(2K_{\mathrm{u}}+1)$ LMI constraints of size 1 and an SOC constraint of size $2N$, then the total number of decision variables is $n_1 = 2N + 1$. Given an accuracy threshold $\epsilon > 0$, the number of iterations required to reach an ϵ-optimal solution is on the order of $\sqrt{\varphi(\mathcal{K}_{\mathcal{A}})} \cdot \ln(1/\epsilon)$, where $\varphi(\mathcal{K}_{\mathcal{A}}) = 2K_{\mathrm{u}} + 3$ is the so-called barrier parameter. In each iteration, the required computational complexity is on the order of $[n_1 \cdot (2K_{\mathrm{u}} + 1) + n_1^2 \cdot (2K_{\mathrm{u}} + 1) + n_1 \cdot (2N)^2 + n_1^3]$, which can be written as $\mathcal{O}\left(N^3 + N^2K_{\mathrm{u}}\right)$. Note that the number of problem $\mathcal{P}_3$ to be solved is N_{p}, depending on the number of convex sub-sets, then the computational complexity of the proposed symbol-scaling CI-SLP scheme

through solving problem $\mathcal{P}_3$ with CVX is on the order of $N_{\rm p}\ln(1/\epsilon)\cdot\sqrt{2K_{\rm u}+3}\cdot\mathcal{O}\left(N^3+N^2K_{\rm u}\right)$.

Next, we analyze the computational complexity of solving problem $\mathcal{P}_5$ by the proposed efficient algorithm given in Algorithm 2 with the modified Hooke-Jeeves pattern search method summarized in Algorithm 1. In Algorithm 1, the maximum number of iterations is set as $N_{\max}$. In each iteration, we need to calculate $\mathcal{F}\left(\boldsymbol{\lambda}_y^i \pm d\mathbf{u}_i\right)$ $4K_{\rm u}$ times, and each time with computational complexity order of $4NK_{\rm u}$. Therefore, the computational complexity of solving problem $\mathcal{P}_5$ by the Hooke-Jeeves pattern search algorithm is on the order of $N_{\max}\cdot 4K_{\rm u}\cdot(4NK_{\rm u})$. Further considering that problem $\mathcal{P}_5$ needs to be solved $N_{\rm p}$ times, then the computational complexity of the proposed symbol-scaling CI-SLP scheme solved by the efficient algorithm with the Hooke-Jeeves pattern search method is on the order of $16N_{\rm p}N_{\max}\left(NK_{\rm u}^2\right)$, which can be written as $N_{\rm p}N_{\max}\mathcal{O}\left(NK_{\rm u}^2\right)$ and is much lower than that solved by CVX especially the fact that $K_{\rm u}\leq N$.

To further improve the efficiency of the proposed precoding scheme, we also attempt to simplify $\mathcal{P}_3$ as a weighted optimization problem, which treat the radar sensing constraint (20b) as a weighted penalty in the objective function. In this way, problem $\mathcal{P}_3$ can be further transformed into a QP optimization problem and can be solved more effectively. The detailed design method is presented in the following section.

IV. Weighted Symbol-Scaling CI-SLP Design for ISAC

A. Weighted Optimization Problem

In order to further improve the efficiency of the proposed symbol-scaling CI-SLP for ISAC with flexible control on the communication and radar performance, we further incorporate the radar constraint (20b) in the objective function, constructing a weighted optimization problem for ISAC. The weighted optimization problem can be written as

$$\begin{aligned}\mathcal{P}_6:\ \min_{t,\mathbf{x}_{\rm E}}\ & (1-\rho)\left(-\xi t\right)+\rho\left(-\mathbf{c}^{\rm T}\mathbf{x}_{\rm E}\right) && (32)\\ \text{s.t.}\ \ & \mathbf{M}\mathbf{x}_{\rm E}\geq t\cdot\mathbf{1}, && (32a)\\ & \|\mathbf{x}_{\rm E}\|_2^2\leq p_0, && (32b)\end{aligned}$$

where $0\leq\rho\leq 1$ is the weighting factor that determines the weights for radar performance (with ρ) and communication performance (with $1-\rho$) in the ISAC system. In the objective function of problem $\mathcal{P}_6$, we introduce $\xi>0$ as a regulating factor to balance the values of the communication performance term t and the radar performance term $\mathbf{c}^{\rm T}\mathbf{x}_{\rm E}$, whose value depends on the practical system setting. Problem $\mathcal{P}_6$ is convex and can be solve with CVX directly. In order to gain more insights to the solution of the formulated optimization problem $\mathcal{P}_6$ and further reduce the computational complexity, we also try to leverage the Lagrangian method to solve the problem.

B. Closed-Form Structure for $\mathbf{x}_{\rm E}$

We analyze $\mathcal{P}_6$ based on the Lagrangian and KKT conditions to derive the optimal transmit signal vector $\mathbf{x}_{\rm E}$. The Lagrangian function of $\mathcal{P}_6$ can be constructed as

$$\begin{aligned}\mathcal{L}\left(\mathbf{x}_{\rm E},t,\boldsymbol{\lambda},\mu\right)=&-\left(1-\rho\right)\xi t-\rho\left(\mathbf{c}^{\rm T}\mathbf{x}_{\rm E}\right)\\&+\boldsymbol{\lambda}^{\rm T}\left(t\cdot\mathbf{1}-\mathbf{M}\mathbf{x}_{\rm E}\right)+\mu\left(\|\mathbf{x}_{\rm E}\|_2^2-p_0\right),\end{aligned}\tag{33}$$

where $\boldsymbol{\lambda}$ and μ are the non-negative dual variables associated with the inequality constraints (32a) and (32b) respectively. Accordingly, the KKT conditions for the optimality of $\mathcal{P}_6$ can be formulated as

$$\frac{\partial\mathcal{L}}{\partial t}=\mathbf{1}^{\rm T}\boldsymbol{\lambda}-\left(1-\rho\right)\xi=0,\tag{34a}$$

$$\frac{\partial\mathcal{L}}{\partial\mathbf{x}_{\rm E}}=-\rho\mathbf{c}-\mathbf{M}^{\rm T}\boldsymbol{\lambda}+2\mu\mathbf{x}_{\rm E}=0,\tag{34b}$$

$$\boldsymbol{\lambda}^{\rm T}\left(t\cdot\mathbf{1}-\mathbf{M}\mathbf{x}_{\rm E}\right)=0,\ \lambda_k\geq 0,\ \forall k\leq 2K_{\rm u},\tag{34c}$$

$$\mu\left(\|\mathbf{x}_{\rm E}\|_2^2-p_0\right)=0,\ \mu\geq 0.\tag{34d}$$

Similar to the situation in Section III-C, we can first obtain that $\mu>0$, otherwise there is no $\boldsymbol{\lambda}$ that satisfies (34b). This means that the total power constraint (32b) is active when the optimality is achieved, i.e.,

$$\|\mathbf{x}_{\rm E}\|_2^2=p_0.\tag{35}$$

To proceed, we can further transform (34b) into

$$\mathbf{x}_{\rm E}=\frac{1}{2\mu}\left(\rho\mathbf{c}+\mathbf{M}^{\rm T}\boldsymbol{\lambda}\right),\tag{36}$$

which is a closed-form structure for the optimal transmit signal vector $\mathbf{x}_{\rm E}$ as a function of the Lagrange multipliers $\boldsymbol{\lambda}$ and μ.

C. Dual Problem Formulation

It is obvious that the Slaters condition is satisfied for the convex optimization problem $\mathcal{P}_6$ [37]. Accordingly, we can solve $\mathcal{P}_6$ optimally by solving its dual problem, the corresponding objective is given below

$$\max_{\boldsymbol{\lambda},\mu}\min_{\mathbf{x}_{\rm E},t}\mathcal{L}\left(\mathbf{x}_{\rm E},t,\boldsymbol{\lambda},\mu\right),\tag{37}$$

where the optimal solution is achieved with the KKT condition (34a), the active total power constraint in (35) and the optimal structure of $\mathbf{x}_{\rm E}$ in (36). By substituting (34a), (35) and (36) into (37), the objective function of the dual problem can be simplified and given by

$$\begin{aligned}&\max_{\boldsymbol{\lambda},\mu}\min_{\mathbf{x}_{\rm E},t}\mathcal{L}\left(\mathbf{x}_{\rm E},t,\boldsymbol{\lambda},\mu\right)\\=&\max_{\boldsymbol{\lambda},\mu}\min_{\mathbf{x}_{\rm E},t}-\left(1-\rho\right)\xi t-\rho\left(\mathbf{c}^{\rm T}\mathbf{x}_{\rm E}\right)+\boldsymbol{\lambda}^{\rm T}\left(t\cdot\mathbf{1}-\mathbf{M}\mathbf{x}_{\rm E}\right)\\&\qquad+\mu\left(\|\mathbf{x}_{\rm E}\|_2^2-p_0\right)\\=&\min_{\boldsymbol{\lambda},\mu}\frac{1}{2\mu}\left(\rho\cdot\mathbf{c}^{\rm T}+\boldsymbol{\lambda}^{\rm T}\mathbf{M}\right)\left(\rho\mathbf{c}+\mathbf{M}^{\rm T}\boldsymbol{\lambda}\right)\\=&\min_{\boldsymbol{\lambda},\mu}\frac{1}{2\mu}\left(\boldsymbol{\lambda}^{\rm T}\mathbf{M}\mathbf{M}^{\rm T}\boldsymbol{\lambda}+2\rho\mathbf{c}^{\rm T}\mathbf{M}^{\rm T}\boldsymbol{\lambda}+\rho^2\mathbf{c}^{\rm T}\mathbf{c}\right).\end{aligned}\tag{38}$$

By substituting (36) into (35), the total power constraint is equivalent to

$$\begin{aligned}&\frac{1}{4\mu^2}\left(\rho\mathbf{c}+\mathbf{M}^{\rm T}\boldsymbol{\lambda}\right)^{\rm T}\left(\rho\mathbf{c}+\mathbf{M}^{\rm T}\boldsymbol{\lambda}\right)=p_0\\\Rightarrow&\frac{1}{4\mu^2}\left(\boldsymbol{\lambda}^{\rm T}\mathbf{M}\mathbf{M}^{\rm T}\boldsymbol{\lambda}+2\rho\mathbf{c}^{\rm T}\mathbf{M}^{\rm T}\boldsymbol{\lambda}+\rho^2\mathbf{c}^{\rm T}\mathbf{c}\right)=p_0.\end{aligned}\tag{39}$$

Then we can obtain the following expression for μ:

$$\mu = \sqrt{\frac{\left(\boldsymbol{\lambda}^{\mathrm{T}}\mathbf{M}\mathbf{M}^{\mathrm{T}}\boldsymbol{\lambda} + 2\rho\mathbf{c}^{\mathrm{T}}\mathbf{M}^{\mathrm{T}}\boldsymbol{\lambda} + \rho^2\mathbf{c}^{\mathrm{T}}\mathbf{c}\right)}{4p_0}}. \tag{40}$$

Substituting the above expression for μ into (38), the objective of the dual problem can be further transformed into an optimization on $\boldsymbol{\lambda}$ only, given by

$$\begin{aligned}
&\min_{\boldsymbol{\lambda},\mu} \frac{1}{2\mu}\left(\boldsymbol{\lambda}^{\mathrm{T}}\mathbf{M}\mathbf{M}^{\mathrm{T}}\boldsymbol{\lambda} + 2\rho\mathbf{c}^{\mathrm{T}}\mathbf{M}^{\mathrm{T}}\boldsymbol{\lambda} + \rho^2\mathbf{c}^{\mathrm{T}}\mathbf{c}\right) \\
=&\min_{\boldsymbol{\lambda}} \frac{\left(\boldsymbol{\lambda}^{\mathrm{T}}\mathbf{M}\mathbf{M}^{\mathrm{T}}\boldsymbol{\lambda} + 2\rho\mathbf{c}^{\mathrm{T}}\mathbf{M}^{\mathrm{T}}\boldsymbol{\lambda} + \rho^2\mathbf{c}^{\mathrm{T}}\mathbf{c}\right)}{2\sqrt{\frac{\left(\boldsymbol{\lambda}^{\mathrm{T}}\mathbf{M}\mathbf{M}^{\mathrm{T}}\boldsymbol{\lambda} + 2\rho\mathbf{c}^{\mathrm{T}}\mathbf{M}^{\mathrm{T}}\boldsymbol{\lambda} + \rho^2\mathbf{c}^{\mathrm{T}}\mathbf{c}\right)}{4p_0}}} \\
=&\min_{\boldsymbol{\lambda}} \sqrt{p_0\left(\boldsymbol{\lambda}^{\mathrm{T}}\mathbf{M}\mathbf{M}^{\mathrm{T}}\boldsymbol{\lambda} + 2\rho\mathbf{c}^{\mathrm{T}}\mathbf{M}^{\mathrm{T}}\boldsymbol{\lambda} + \rho^2\mathbf{c}^{\mathrm{T}}\mathbf{c}\right)} \\
=&\min_{\boldsymbol{\lambda}} \boldsymbol{\lambda}^{\mathrm{T}}\mathbf{M}\mathbf{M}^{\mathrm{T}}\boldsymbol{\lambda} + 2\rho\mathbf{c}^{\mathrm{T}}\mathbf{M}^{\mathrm{T}}\boldsymbol{\lambda},
\end{aligned} \tag{41}$$

where the last step is achieved because $f(x) = \sqrt{x}$ is a monotonic function versus x and thus the optimal solution for minimizing $\sqrt{x}$ is equivalent to minimizing x. Accordingly, the final dual problem of the proposed weighted optimization can be formulated as

$$\mathcal{P}_7: \min_{\boldsymbol{\lambda}} \boldsymbol{\lambda}^{\mathrm{T}}\mathbf{M}\mathbf{M}^{\mathrm{T}}\boldsymbol{\lambda} + 2\rho\mathbf{c}^{\mathrm{T}}\mathbf{M}^{\mathrm{T}}\boldsymbol{\lambda} \tag{42}$$

$$\text{s.t.} \quad \mathbf{1}^{\mathrm{T}}\boldsymbol{\lambda} - (1-\rho)\,\xi = 0, \tag{42a}$$

$$\lambda_k \geq 0, \ \forall 1 \leq k \leq 2K_{\mathrm{u}}. \tag{42b}$$

Note that $\mathcal{P}_7$ is a QP optimization problem over a simplex, which can be more efficiently solved than the optimization problem $\mathcal{P}_3$ and the weighted optimization problem $\mathcal{P}_6$ via the standard simplex method [40], the interior-point methods [41] or alternating direction method of multipliers [42]. After solving $\mathcal{P}_7$ and obtaining μ^* and $\mathbf{x}_{\mathrm{E}}^*$ via (40) and (36), the corresponding t^* can be obtained achieved through (30). The proposed weighted symbol-scaling SLP for ISAC can be summarized by the following Algorithm 3.

Algorithm 3 Weighted Symbol-Scaling CI-SLP Design for ISAC

1: **Input**: $\mathbf{s}_k[l]$, $\mathbf{H} = [\mathbf{h}_1, \cdots, \mathbf{h}_{K_{\mathrm{u}}}]^{\mathrm{T}}$, $\mathbf{a}(\theta)$, p_0, ρ
2: Initial $\mathbf{M}$, $\mathbf{a}_{\mathrm{E}}$ and $\mathbf{b}_{\mathrm{E}}$;
3: Select a group of approximate feasible domains;
4: Solve N_{p} optimization problems $\mathcal{P}_7$ with specific $\mathbf{c}$ and d according to the composition of the feasible domain and obtain $\left\{\boldsymbol{\lambda}_1^*, \cdots, \boldsymbol{\lambda}_{N_{\mathrm{p}}}^*\right\}$;
5: Compute $\left\{\left\{\mu_1^*, \mathbf{x}_{\mathrm{E},1}^*, t_1^*\right\}, \cdots, \left\{\mu_{N_{\mathrm{p}}}^*, \mathbf{x}_{\mathrm{E},N_{\mathrm{p}}}^*, t_{N_{\mathrm{p}}}^*\right\}\right\}$ by (40), (36) and (30);
6: Find the global optimal solution $\mathbf{x}_{\mathrm{E}}^*$ by (21);
7: Obtain the transmit signal vector $\mathbf{x}[l]$ by (31).
8: **Output**: $\mathbf{x}[l]$

D. Complexity Analysis

The computational complexity of the proposed Algorithm 3 for solving the weighted problem $\mathcal{P}_6$ mainly comes from solving the dual problem $\mathcal{P}_7$. Since $\mathcal{P}_6$ and $\mathcal{P}_7$ are convex optimization problems and only involve LMI and SOC constraints, they can both be solved with standard IPM with CVX. In the following, we will analyze these two problems sequentially.

First, considering that $\mathcal{P}_6$ has $2K_{\mathrm{u}}$ LMI constraints of size 1 and an SOC constraint of size $2N$, the number of decision variables is $n_2 = 2N + 1$. Also, the number of iterations required to reach an ϵ-optimal solution is on the order of $\sqrt{\varphi(\mathcal{K}_{\mathcal{B}})} \cdot \ln(1/\epsilon)$, where $\varphi(\mathcal{K}_{\mathcal{B}}) = 2K_{\mathrm{u}} + 2$. In each iteration, the required computational complexity is on the order of $[n_2 \cdot 2K_{\mathrm{u}} + n_2^2 \cdot 2K_{\mathrm{u}} + n_2 \cdot (2N)^2 + n_2^3]$, which can be written as $\mathcal{O}\left(N^3 + N^2K_{\mathrm{u}}\right)$. Further considering that problem $\mathcal{P}_6$ needs to be solved N_{p} times, the computational complexity of the proposed weighted symbol-scaling CI-SLP scheme through solving problem $\mathcal{P}_6$ with CVX is on the order of $N_{\mathrm{p}}\ln(1/\epsilon) \cdot \sqrt{2K_{\mathrm{u}} + 2} \cdot \mathcal{O}\left(N^3 + N^2K_{\mathrm{u}}\right)$.

Next, consider $\mathcal{P}_7$, which only has $(2K_{\mathrm{u}} + 1)$ LMI constraints of size 1 and the number of decision variables is $n_3 = 2K_{\mathrm{u}}$. Also, the number of iterations required to reach an ϵ-optimal solution is on the order of $\sqrt{\varphi(\mathcal{K}_{\mathcal{C}})} \cdot \ln(1/\epsilon)$, where $\varphi(\mathcal{K}_{\mathcal{C}}) = 2K_{\mathrm{u}} + 1$. In each iteration, the required computational complexity is on the order of $[n_3 \cdot (2K_{\mathrm{u}} + 1) + n_3^2 \cdot (2K_{\mathrm{u}} + 1) + n_3^3]$, which can be written as $\mathcal{O}\left(K_{\mathrm{u}}^3\right)$. Hence, the computational complexity of the proposed weighted symbol-scaling CI-SLP scheme through solving problem $\mathcal{P}_7$ with the Algorithm 3 is on the order of $N_{\mathrm{p}}\ln(1/\epsilon) \cdot \sqrt{2K_{\mathrm{u}} + 1} \cdot \mathcal{O}\left(K_{\mathrm{u}}^3\right)$, which is much lower than solving problem $\mathcal{P}_6$ directly with CVX, especially considering the fact that $K_{\mathrm{u}} \leq N$.

V. Extension to Block-Level Precoding

The above symbol-scaling precoding schemes for ISAC are based on CI-SLP. Furthermore, CI-BLP approaches can offer an improved ISAC performance compared with traditional CI-SLP approaches thanks to the relaxed block-level total power constraint, which meanwhile reduce the update frequency of the precoder as the optimization problem only needs to be solved once per block [34]. In order to be more consistent with the currently used communication systems and achieve better ISAC performance, we consider extending the proposed CI-SLP design to CI-BLP.

Fig. 4 depicts the difference between the conventional BLP, CI-SLP and CI-BLP. Compared to CI-SLP approaches that optimize the transmit signals on a symbol level, CI-BLP scheme can reduce the update frequency of the precoder because the optimization only needs to be performed once per block of symbol slots. Compared to conventional BLP, CI-SLP and CI-BLP can achieve better performance by designing the data-dependent precoding. The application of symbol-scaling CI-SLP in ISAC system has been derived previously in Sections III, and the design for CI-BLP will be presented directly below.

First, we define

$$\hat{\boldsymbol{\alpha}}_{\mathrm{E}} = \left[\boldsymbol{\alpha}_{\mathrm{E}}[1]^{\mathrm{T}}, \boldsymbol{\alpha}_{\mathrm{E}}[2]^{\mathrm{T}}, \cdots, \boldsymbol{\alpha}_{\mathrm{E}}[L]^{\mathrm{T}}\right]^{\mathrm{T}} \in \mathbb{R}^{2LK_{\mathrm{u}} \times 1}, \tag{43}$$

$$\hat{\mathbf{x}}_{\mathrm{E}} = \left[\mathbf{x}_{\mathrm{E}}[1]^{\mathrm{T}}, \mathbf{x}_{\mathrm{E}}[2]^{\mathrm{T}}, \cdots, \mathbf{x}_{\mathrm{E}}[L]^{\mathrm{T}}\right]^{\mathrm{T}} \in \mathbb{R}^{2LN \times 1}, \tag{44}$$

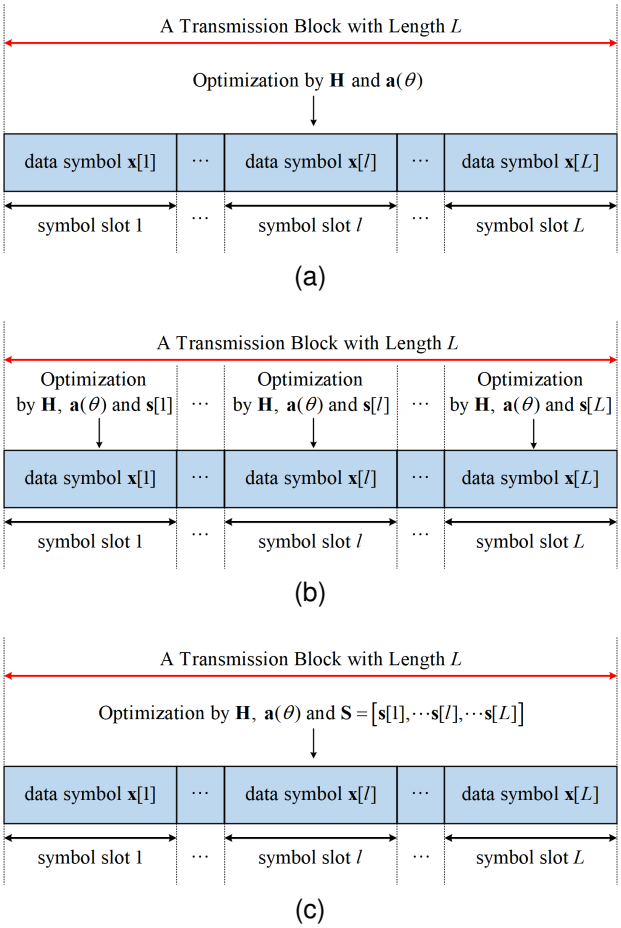

Fig. 4. (a) Conventional BLP. (b) CI-SLP. (c) CI-BLP.

$$\hat{\mathbf{M}}=\begin{bmatrix}\mathbf{M}[1] & & & \\ & \mathbf{M}[2] & & \\ & & \ddots & \\ & & & \mathbf{M}[L]\end{bmatrix}\in\mathbb{R}^{2LK_{\mathrm{u}}\times 2LN}, \quad (45)$$

where $\boldsymbol{\alpha}_{\mathrm{E}}[l]$, $\mathbf{x}_{\mathrm{E}}[l]$ and $\mathbf{M}[l]$ respectively represent $\boldsymbol{\alpha}_{\mathrm{E}}$, $\mathbf{x}_{\mathrm{E}}$ and $\mathbf{M}$ in the l-th time slot in the above derivation. L represents the length of the considered block which is smaller than the channel coherence interval. With the above definition, the original optimization problem $\mathcal{P}_0$ at the symbol level can be extended to the block level:

$$\begin{aligned}\mathcal{P}_0^{\mathrm{BLP}}:\ &\max_{\hat{\mathbf{x}}_{\mathrm{E}}}\ \min_{i}\ \alpha_i && (46)\\ &\text{s.t.}\ \ \hat{\boldsymbol{\alpha}}_{\mathrm{E}}=\hat{\mathbf{M}}\hat{\mathbf{x}}_{\mathrm{E}}, && (46a)\\ &\quad \left|\mathbf{a}_{\mathrm{E},\mathrm{k_t}}^{\mathrm{T}}\mathbf{x}_{\mathrm{E}}[l]\right|^2+\left|\mathbf{b}_{\mathrm{E},\mathrm{k_t}}^{\mathrm{T}}\mathbf{x}_{\mathrm{E}}[l]\right|^2\geq\hat{p}_r,\forall l\leq L, && (46b)\\ &\quad \|\hat{\mathbf{x}}_{\mathrm{E}}\|_2^2\leq L\cdot p_0, && (46c)\end{aligned}$$

where the total power budget is enforced over the entire considered block instead of within each symbol slot as shown in (46c), i.e., a relaxed total power constraint is enforced compared to the CI-SLP scheme.

By following a similar procedure as that in Section III-B, problem $\mathcal{P}_2$ at the symbol level can also be extended to the block level, written as

$$\begin{aligned}\mathcal{P}_1^{\mathrm{BLP}}:\ &\min_{t,\hat{\mathbf{x}}_{\mathrm{E}}}\ -t && (47)\\ &\text{s.t.}\ \ \hat{\mathbf{M}}\hat{\mathbf{x}}_{\mathrm{E}}\geq t\cdot\mathbf{1}, && (47a)\\ &\quad \mathbf{c}_l^{\mathrm{T}}\mathbf{x}_{\mathrm{E}}[l]\geq d_l,\forall l\leq L, && (47b)\\ &\quad \|\hat{\mathbf{x}}_{\mathrm{E}}\|_2^2\leq L\cdot p_0, && (47c)\end{aligned}$$

where the values of $\mathbf{c}_l$ and d_l are determined in the same way as the values of $\mathbf{c}$ and d in $\mathcal{P}_2$. By defining $\hat{\mathbf{C}}\in\mathbb{R}^{L\times 2LN}$ and $\hat{\mathbf{d}}\in\mathbb{R}^{L\times 1}$ as

$$\hat{\mathbf{C}}=\begin{bmatrix}\mathbf{c}_1^{\mathrm{T}} & & & \\ & \mathbf{c}_2^{\mathrm{T}} & & \\ & & \ddots & \\ & & & \mathbf{c}_L^{\mathrm{T}}\end{bmatrix},\quad \hat{\mathbf{d}}=[d_1,d_2,\cdots,d_L]^{\mathrm{T}}, \quad (48)$$

problem $\mathcal{P}_1^{\mathrm{BLP}}$ can be further rewritten as

$$\begin{aligned}\mathcal{P}_2^{\mathrm{BLP}}:\ &\min_{t,\hat{\mathbf{x}}_{\mathrm{E}}}\ -t && (49)\\ &\text{s.t.}\ \ \hat{\mathbf{M}}\hat{\mathbf{x}}_{\mathrm{E}}\geq t\cdot\mathbf{1}, && (49a)\\ &\quad \hat{\mathbf{C}}\hat{\mathbf{x}}_{\mathrm{E}}\geq\hat{\mathbf{d}}, && (49b)\\ &\quad \|\hat{\mathbf{x}}_{\mathrm{E}}\|_2^2\leq L\cdot p_0. && (49c)\end{aligned}$$

In problem $\mathcal{P}_2^{\mathrm{BLP}}$, the transmit signals in L time slots are combined into a whole vector $\hat{\mathbf{x}}_{\mathrm{E}}$ as the optimization variable, which enables the optimization to be performed at the block level. In the CI-BLP ISAC problem, after obtaining the globally optimal $\hat{\mathbf{x}}_{\mathrm{E}}^*$, the transmit signal vector for each symbol slot can be obtained according to (44) by a similar matrix operation as (31).

VI. Simulation Results

In this section, we present numerical results to validate the above derivations and illustrate the superiority of the proposed approach. The proposed schemes are compared with PDD-MM-BCD in [29] in terms of SER performance, transmit beampattern and execution time. The execution time results are obtained from a Windows 11 Desktop with i5-12400 and 16GB RAM.

The following abbreviations for the simulated schemes are used throughout this section:

1) PDD-MM-BCD: PDD-MM-BCD in [29], which is an CI-SLP scheme based on the penalty dual decomposition (PDD), majorization-minimization (MM), and block coordinate descent (BCD) methods for ISAC system.
2) SS-SLP-4D/8D: The proposed CI-SLP based on symbol scaling summarized in Algorithm 2, with the first/second group of feasible domains.
3) Weighted-SLP-4D/8D: The proposed weighted CI-SLP based on symbol scaling summarized in Algorithm 3, with the first/second group of feasible domains.
4) SS-BLP-4D/8D: The proposed CI-BLP based on symbol scaling, with the first/second group of feasible domains.

Although the PDD-MM-BCD scheme in [29] considers constant modulus constraint, we relaxed the constant modulus constraint of PDD-MM-BCD scheme to total power constraint in the simulations for fairness. The PDD-MM-BCD scheme is

a double-loop algorithm, in which the outer loop is used to approximate the constant modulus constraint. Under the total power constraint, the PDD-MM-BCD scheme only needs to perform the inner loop, thus reducing part of the computational complexity. Throughout the simulations, the transmit power budget per symbol slot is set as $p_0 = 30$dBm, and QPSK modulation is employed. The BS is equipped with N antennas with antenna spacing $\Delta = \frac{\lambda}{2}$ where λ is the wavelength of the carrier signal. We set the QoS for communication requirement of the PDD-MM-BCD scheme as $\beta_{\mathrm{c}} = \sigma_{\mathrm{c}}\Gamma_{\mathrm{c}}$, where $\sigma_{\mathrm{c}} = 22$dBm and $\Gamma_{\mathrm{c}} = 2.2$dB . In the SS-SLP scheme proposed in this paper, we assume that the illumination power requirement for each target is $p_{\mathrm{r},k_{\mathrm{t}}} = \sigma_{\mathrm{r}}^2\Gamma_{\mathrm{r}}$, where $\sigma_{\mathrm{r}}^2 = 20$dBm. In the Weighted-SLP scheme proposed in this paper, the regulating factor is $\xi = 3.33$.

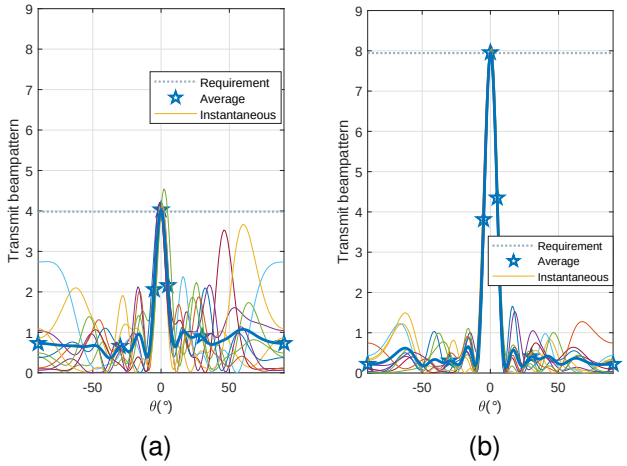

Fig. 5. Transmit beampatterns of the proposed SS-SLP scheme, $N = 10$, $K_{\mathrm{u}} = 3$. (a) $\Gamma_{\mathrm{r}} = 16$dB. (b) $\Gamma_{\mathrm{r}} = 19$dB.

In this paper, we take the illumination power towards the target as the radar constraint. This simple radar constraint may indeed result in a suboptimal instantaneous beampattern with certain sidelobe. However, the sidelobe of the average beampattern with a large number of samples is acceptable, because the sidelobes of different time slots are quite random in the strength and width. We simulate the proposed SS-SLP scheme with radar thresholds Γ_{r} of 16dB and 19dB, as shown in Fig. 5. The number of transmit antennas is $N = 10$, the number of users is $K_{\mathrm{u}} = 3$, and the target is at the location $\theta_1 = 0°$ with $\beta_1 = 1$. We present the instantaneous beampattern for each of the 10 time slots as well as their average beampattern. It can be seen that the sidelobe of the average beampattern of 10 samples is acceptable. The subsequent results are all average results, which is also reasonable in practical ISAC system. In addition, intuitively, we try to maximize the mainlobe power, and the sidelobe power can be suppressed through appropriate beampattern design considering the limited total power. Fig. 5(a) shows the instantaneous beampatterns and their average beampattern with low illumination power requirement. Fig. 5(b) shows the instantaneous beampatterns and their average beampattern when the illumination power requirement becomes demanding, and it can be seen that the sidelobes can be better suppressed. Therefore, we can also obtain a satisfactory peak side lobe ratio (PSLR) by selecting a higher radar threshold.

This simple radar constraint will lead to undesirable instantaneous sidelobes. However, the average sidelobe of multiple samples is acceptable, because the sidelobe of different samples varies greatly. Fig. 5 depict the instantaneous beampatterns of the proposed SS-SLP scheme, when $N = 10$, $K_{\mathrm{u}} = 3$, and the target at the location $\theta_1 = 0°$ with $\beta_1 = 1$. Fig. 5(a) shows the instantaneous beampatterns and their average beampattern with low illumination power requirement. Fig. 5(b) shows the instantaneous beampatterns and their average beampattern when the illumination power requirement becomes demanding, and it can be seen that the sidelobes have been better suppressed. The subsequent results are all average results, which is also reasonable in practical ISAC system.

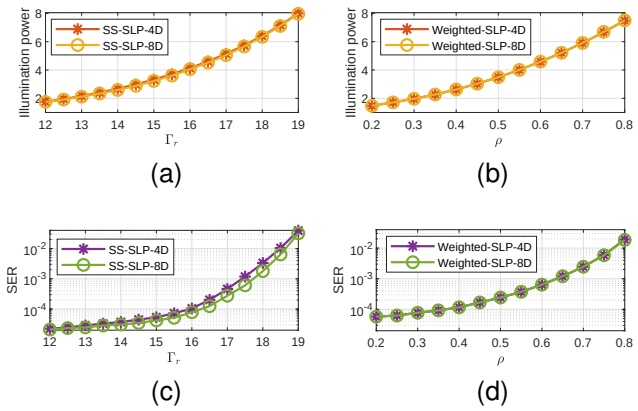

Fig. 6. The effect of Γ_{r} on the SS-SLP scheme and ρ on the Weighted-SLP scheme, $N = 10$, $K_{\mathrm{u}} = 3$. (a) illumination power towards the target versus Γ_{r}. (b) illumination power towards the target versus ρ. (c) SER versus Γ_{r}. (d) SER versus ρ.

The effect of Γ_{r} on the SS-SLP scheme and ρ on the Weighted-SLP scheme are first plotted, respectively, when $N = 10$, $K_{\mathrm{u}} = 3$, and the target at the location $\theta_1 = 0°$ with $\beta_1 = 1$. In such a system, the ISAC performance of the SS-SLP scheme corresponding to different Γ_{r} is shown in Fig. 6(a) and 6(c), while the ISAC performance of the Weighted-SLP scheme corresponding to different ρ is shown in Fig. 6(b) and 6(d). In Fig. 6(a) and 6(c), a larger Γ_{r} means a higher requirement for illumination power towards the target, and at the same time the SER performance for communication will be worse. Similarly, in Fig. 6(b) and 6(d), larger ρ means better radar performance and worse communication performance.

Fig. 7 and Fig. 8 respectively depict the SER performance and transmit beampatterns of different schemes, when $N = 10$, $K_{\mathrm{u}} = 3$, and the target at the location $\theta_1 = 0°$ with $\beta_1 = 1$. In this scenario, we set $\Gamma_{\mathrm{r}} = 18.4$dB and $\rho = 0.8$. When the transmit beampatterns are similar, the proposed CI-SLP ISAC schemes based on symbol scaling can obtain better SER performance under the constraint of the second group of feasible domains, because the second group of feasible domains is closer to the original feasible domains. SS-SLP constrained by the first and the second groups of feasible

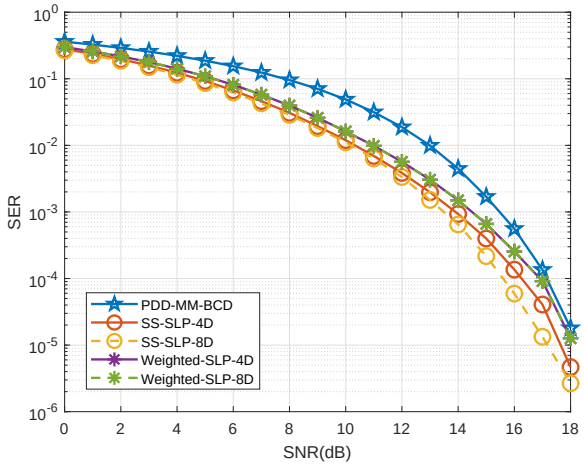

Fig. 7. SER performance of different schemes, $N = 10$, $K_{\mathrm{u}} = 3$.

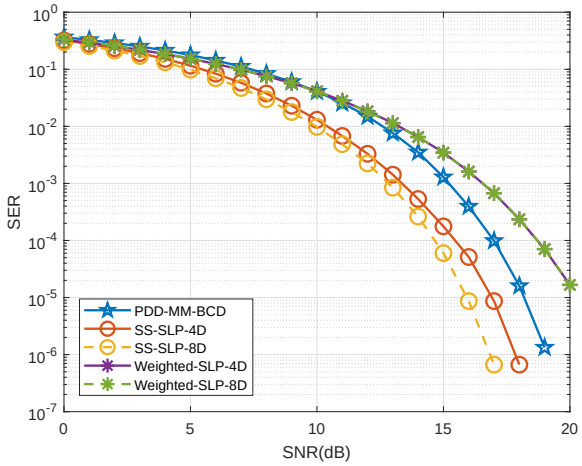

Fig. 9. SER performance of different schemes, $N = 10$, $K_{\mathrm{u}} = 3$, $K_{\mathrm{t}} = 3$.

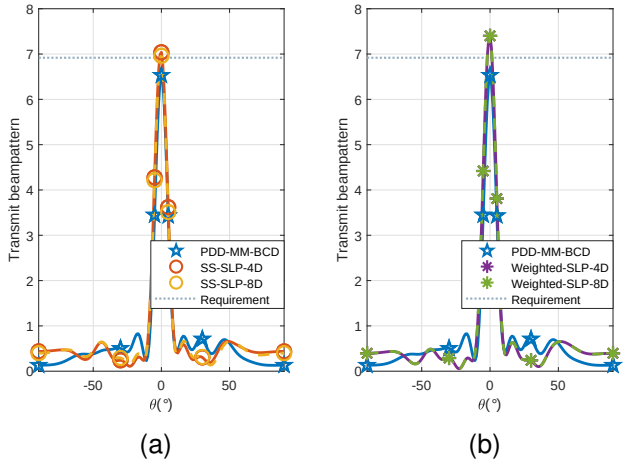

Fig. 8. Transmit beampatterns of different schemes, $N = 10$, $K_{\mathrm{u}} = 3$.

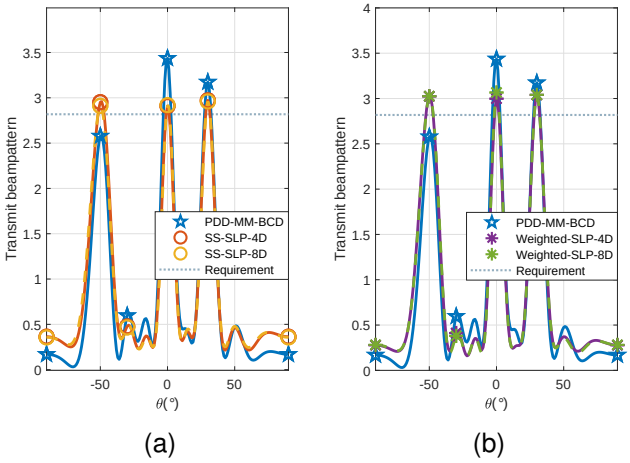

Fig. 10. Transmit beampatterns of different schemes, $N = 10$, $K_{\mathrm{u}} = 3$, $K_{\mathrm{t}} = 3$.

domains can achieve better SER performance than PDD-MM-BCD, which shows the advantages of our proposed CI-SLP ISAC schemes based on symbol scaling. At the same time, the Weighted-SLP schemes also perform significantly better than PDD-MM-BCD under the constraints of the first and the second groups of feasible domains, thanks to the fact that the objective function in the optimization problem does not require approximation. For SS-SLP and Weighted-SLP, the results of taking the first and the second groups of feasible domains are very close, indicating that these two groups of feasible domains are closely approaching the original non-convex feasible domains.

Fig. 9 and Fig. 10 respectively show the SER performance and transmit beampatterns of different schemes, when multiple targets are detected simultaneously, with $N = 10$, $K_{\mathrm{u}} = 3$. We assume there are $K_{\mathrm{t}} = 3$ targets at the locations $\theta_1 = -50°$, $\theta_2 = 0°$, and $\theta_3 = 30°$, respectively, with the same amplitudes $\beta_1 = \beta_2 = \beta_3 = 1$. In this scenario, we set $\Gamma_{\mathrm{r}} = 14.5$dB and $\rho = 0.8$. The SER results for multi-target detection are similar to those for single-target detection. By observing Fig. 10(a), it can be seen that when the target positions are asymmetrical, the illumination power of different targets in PDD-MM-BCD scheme is quite different, while the illumination power of different targets in SS-SLP scheme is almost the same. This is because the proposed SS-SLP scheme can impose specific constraints on the illumination power of each target separately, which also indicates that the SS-SLP scheme will be more flexible in practical applications. In Fig. 10(b), there are some differences in the illumination power of different targets in Weighted-SLP scheme, because the original target illumination power constraint is not strictly satisfied in the weighted problem.

Fig. 11 and Fig. 12 respectively depict the SER performance and transmit beampatterns of SLP and BLP, when $N = 10$, $K_{\mathrm{u}} = 3$, and the target at the location $\theta_1 = 0°$ with $\beta_1 = 1$. In the simulation, we set the length of the considered block for BLP as $L = 2$. It can be observed that the transmit beampatterns of SS-BLP scheme and SS-SLP scheme are basically the same. It is obvious that the larger the L, the more obvious advantage for the SER performance of the SS-BLP scheme. When $L = 2$, SS-BLP's SER performance

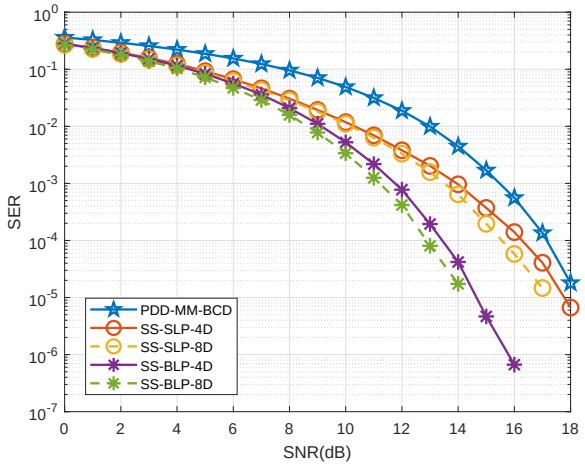

Fig. 11. SER performance of different schemes, $N = 10$, $K_{\mathrm{u}} = 3$.

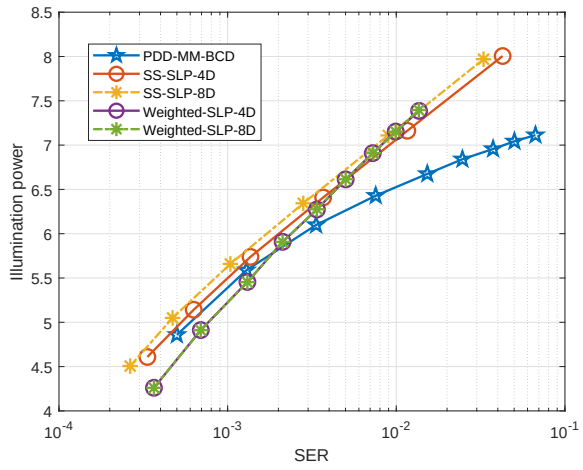

Fig. 13. Tradeoff results of different schemes, $N = 10$, $K_{\mathrm{u}} = 3$.

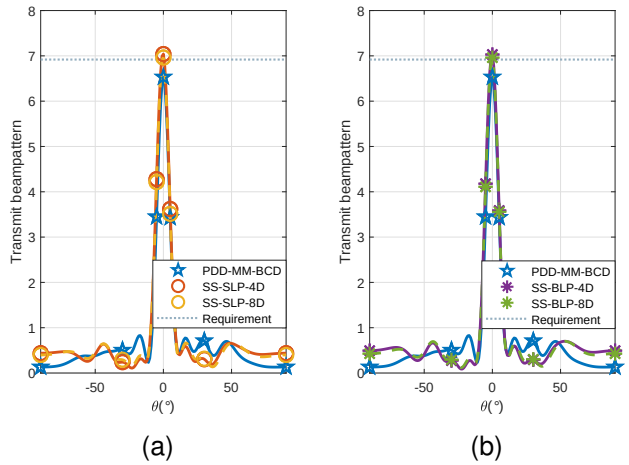

Fig. 12. Transmit beampatterns of different schemes, $N = 10$, $K_{\mathrm{u}} = 3$.

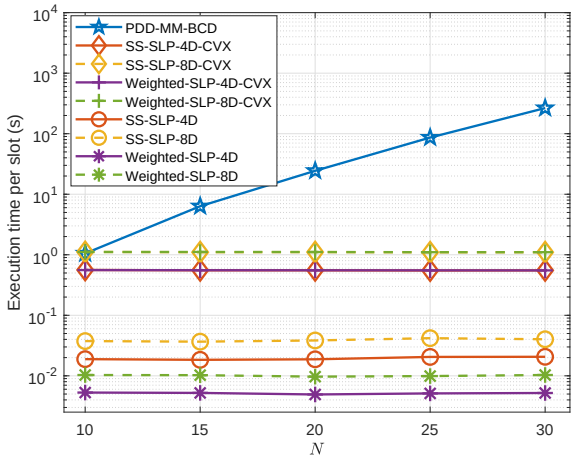

Fig. 14. Execution time of different schemes, $K_{\mathrm{u}} = 3$.

advantage is already significant, thanks to the relaxed total power constraint.

In Fig. 13, we aim to explicitly show the tradeoff results between radar performance and communication performance of different schemes It can be seen that when the radar requirement is high, the proposed SS-SLP scheme and Weighted-SLP scheme have obvious advantages over PDD-MM-BCD, mainly because we adopt different radar performance metrics.

Fig. 14 depicts the complexity of the proposed schemes with PDD-MM-BCD in terms of the execution time. For fairness of comparison, the optimization problems of PDD-MM-BCD, SS-SLP-4D, and SS-SLP-8D are solved by the Hooked-Jeeves pattern search algorithm. The QP problems in Weighted-SLP-4D and Weighted-SLP-8D are solved by quadprog function in MATLAB. In order to better evaluate the efficiency, we include the simulation results of the SS-SLP scheme and Weighed-SLP scheme solved by CVX. SS-SLP-4D-CVX and SS-SLP-8D-CVX represent the results obtained by solving $\mathcal{P}_3$ with CVX. Weighted-SLP-4D-CVX and Weighted-SLP-8D-CVX represent the results obtained by solving $\mathcal{P}_6$ with CVX. It can be seen that compared with the results obtained by CVX, the proposed efficient algorithms of SS-SLP scheme and Weighted-SLP scheme can greatly reduce the execution time, indicating much lower computational complexity. With the increase of the number of transmit antennas, the computational complexity of each scheme will increase correspondingly, because the number of optimization variables in the optimization problem increases. The execution time of CI-SLP ISAC schemes based on symbol scaling is significantly less than PDD-MM-BCD, thanks to the objective function in the original problem that does not require approximation, which eliminates the need for iterative procedures. The execution time of Weighted-SLP is further reduced, thanks to the special construction of the weighted problem, which results in a simple dual problem.

VII. Conclusions

In this paper, we investigate the symbol-scaling based SLP design for ISAC. The SLP design and weighted SLP design based on symbol scaling are proposed. We also extend the scheme proposed in this paper from symbol level to block level. The simulation results show that the proposed SLP

design based on symbol scaling has significant communication performance advantages under the condition of satisfying the radar performance requirements. And as the number of transmit antennas increases, this advantage becomes more obvious. Compared with the previous SLP scheme in ISAC system, the complexity of the proposed scheme is significantly reduced. Motivated by this work, more complicated SLP based ISAC systems deserve further investigation. In addition to the considered target illumination power constraint, this work can be extended to use other radar metrics such as beampattern squared error, mutual information, the Cramer-Rao bound, etc., to explore the performance improvements in radar sensing offered by SLP. Extensions to the CI-BLP as discussed in Section V also warrant further attention.

APPENDIX A
THE CONSTRUCTION OF $\mathbf{M}$

$\mathbf{M}$ in (6) can be constructed based on the channel vector $\mathbf{h}_k$ and the data symbol $\mathbf{s}_k$ for each user, given by

$$\mathbf{M} = \left[\mathbf{p}_1, \mathbf{p}_2, \cdots, \mathbf{p}_{K_\mathrm{u}}, \mathbf{q}_1, \mathbf{q}_2, \cdots, \mathbf{q}_{K_\mathrm{u}}\right]^\mathrm{T} \tag{50}$$

where $\mathbf{p}_k \in \mathbb{R}^{2N\times 1}$ and $\mathbf{q}_k \in \mathbb{R}^{2N\times 1}$ are given by

$$\mathbf{p}_k = \begin{bmatrix} \frac{\Im\left(s_k^{\text{left}}[l]\right)\Re(\mathbf{h}_k) - \Re\left(s_k^{\text{left}}[l]\right)\Im(\mathbf{h}_k)}{\Re\left(s_k^{\text{right}}[l]\right)\Im\left(s_k^{\text{left}}[l]\right) - \Im\left(s_k^{\text{right}}[l]\right)\Re\left(s_k^{\text{left}}[l]\right)} \\ -\frac{\Im\left(s_k^{\text{left}}[l]\right)\Im(\mathbf{h}_k) + \Re\left(s_k^{\text{left}}[l]\right)\Re(\mathbf{h}_k)}{\Re\left(s_k^{\text{right}}[l]\right)\Im\left(s_k^{\text{left}}[l]\right) - \Im\left(s_k^{\text{right}}[l]\right)\Re\left(s_k^{\text{left}}[l]\right)} \end{bmatrix}, \tag{51}$$

and

$$\mathbf{q}_k = \begin{bmatrix} \frac{\Re\left(s_k^{\text{right}}[l]\right)\Im(\mathbf{h}_k) - \Im\left(s_k^{\text{right}}[l]\right)\Re(\mathbf{h}_k)}{\Re\left(s_k^{\text{right}}[l]\right)\Im\left(s_k^{\text{left}}[l]\right) - \Im\left(s_k^{\text{right}}[l]\right)\Re\left(s_k^{\text{left}}[l]\right)} \\ \frac{\Re\left(s_k^{\text{right}}[l]\right)\Re(\mathbf{h}_k) + \Im\left(s_k^{\text{right}}[l]\right)\Im(\mathbf{h}_k)}{\Re\left(s_k^{\text{right}}[l]\right)\Im\left(s_k^{\text{left}}[l]\right) - \Im\left(s_k^{\text{right}}[l]\right)\Re\left(s_k^{\text{left}}[l]\right)} \end{bmatrix}. \tag{52}$$

APPENDIX B
THE VALUES OF $\mathbf{c}$ AND d

The values of $\mathbf{c}$ and d in (19b) for the eight convex sets in the two groups are listed below.

1) For $\left\{\mathbf{x}_\mathrm{E} | r_1 \le -\sqrt{\hat{p}_\mathrm{r}}\right\}$, $\mathbf{c} = -\mathbf{a}_{\mathrm{E},k_\mathrm{t}}$, $d = \sqrt{\hat{p}_\mathrm{r}}$.
2) For $\left\{\mathbf{x}_\mathrm{E} | r_1 \ge \sqrt{\hat{p}_\mathrm{r}}\right\}$, $\mathbf{c} = \mathbf{a}_{\mathrm{E},k_\mathrm{t}}$, $d = \sqrt{\hat{p}_\mathrm{r}}$.
3) For $\left\{\mathbf{x}_\mathrm{E} | r_2 \le -\sqrt{\hat{p}_\mathrm{r}}\right\}$, $\mathbf{c} = -\mathbf{b}_{\mathrm{E},k_\mathrm{t}}$, $d = \sqrt{\hat{p}_\mathrm{r}}$.
4) For $\left\{\mathbf{x}_\mathrm{E} | r_2 \ge \sqrt{\hat{p}_\mathrm{r}}\right\}$, $\mathbf{c} = \mathbf{b}_{\mathrm{E},k_\mathrm{t}}$, $d = \sqrt{\hat{p}_\mathrm{r}}$.
5) For $\left\{\mathbf{x}_\mathrm{E} | r_1 + r_2 \le -\sqrt{2\hat{p}_\mathrm{r}}\right\}$, $\mathbf{c} = -\mathbf{a}_{\mathrm{E},k_\mathrm{t}} - \mathbf{b}_{\mathrm{E},k_\mathrm{t}}$, $d = \sqrt{2\hat{p}_\mathrm{r}}$.
6) For $\left\{\mathbf{x}_\mathrm{E} | r_1 + r_2 \ge \sqrt{2\hat{p}_\mathrm{r}}\right\}$, $\mathbf{c} = \mathbf{a}_{\mathrm{E},k_\mathrm{t}} + \mathbf{b}_{\mathrm{E},k_\mathrm{t}}$, $d = \sqrt{2\hat{p}_\mathrm{r}}$.
7) For $\left\{\mathbf{x}_\mathrm{E} | r_1 - r_2 \le -\sqrt{2\hat{p}_\mathrm{r}}\right\}$, $\mathbf{c} = -\mathbf{a}_{\mathrm{E},k_\mathrm{t}} + \mathbf{b}_{\mathrm{E},k_\mathrm{t}}$, $d = \sqrt{2\hat{p}_\mathrm{r}}$.
8) For $\left\{\mathbf{x}_\mathrm{E} | r_1 - r_2 \ge \sqrt{2\hat{p}_\mathrm{r}}\right\}$, $\mathbf{c} = \mathbf{a}_{\mathrm{E},k_\mathrm{t}} - \mathbf{b}_{\mathrm{E},k_\mathrm{t}}$, $d = \sqrt{2\hat{p}_\mathrm{r}}$.

APPENDIX C
PROOF FOR $\mu > 0$

Assuming $\mu = 0$, $\boldsymbol{\lambda}$ must satisfy (24a) and (24b), as follows

$$\begin{bmatrix} \mathbf{M}^\mathrm{T} \\ \mathbf{1}^\mathrm{T} \end{bmatrix} \boldsymbol{\lambda} = \begin{bmatrix} \nu\mathbf{c} \\ 1 \end{bmatrix}. \tag{53}$$

Based on the expressions of $\mathbf{M}$ in Appendix A and those of $\mathbf{c}$ in Appendix B with $N \ge K_\mathrm{u}$, we know that the matrix $\mathbf{M}$ depends on the channel between the ISAC BS and users while the vector $\mathbf{c}$ depends on the direction of the target, and thus $\mathbf{c}$ is linearly independent with the columns in $\mathbf{M}^\mathrm{T}$ in practice considering the unrelated users and target. Therefore,

$$\begin{aligned} &\mathrm{rank}\left(\begin{bmatrix} \mathbf{M}^\mathrm{T} \\ \mathbf{1}^\mathrm{T} \end{bmatrix}\right) = \min\left\{2N+1, 2K_\mathrm{u}\right\} = 2K_\mathrm{u}, \\ &\mathrm{rank}\left(\begin{bmatrix} \mathbf{M}^\mathrm{T} & \nu\mathbf{c} \\ \mathbf{1}^\mathrm{T} & 1 \end{bmatrix}\right) = \min\left\{2N+1, 2K_\mathrm{u}+1\right\} = 2K_\mathrm{u}+1, \end{aligned} \tag{54}$$

which means there is no solution for $\boldsymbol{\lambda}$. Thus we can obtain $\mu > 0$, which completes the proof.

REFERENCES

[1] L. Zheng, M. Lops, Y. C. Eldar, and X. Wang, "Radar and Communication Coexistence: An Overview: A Review of Recent Methods," *IEEE Signal Process. Mag.*, vol. 36, no. 5, pp. 85–99, 2019.

[2] F. Liu, C. Masouros, A. P. Petropulu, H. Griffiths, and L. Hanzo, "Joint Radar and Communication Design: Applications, State-of-the-Art, and the Road Ahead," *IEEE Trans. Commun.*, vol. 68, no. 6, pp. 3834–3862, 2020.

[3] N. C. Luong, X. Lu, D. T. Hoang, D. Niyato, and D. I. Kim, "Radio Resource Management in Joint Radar and Communication: A Comprehensive Survey," *IEEE Commun. Surveys Tuts.*, vol. 23, no. 2, pp. 780–814, 2021.

[4] J. A. Zhang, M. L. Rahman, K. Wu, X. Huang, Y. J. Guo, S. Chen, and J. Yuan, "Enabling Joint Communication and Radar Sensing in Mobile NetworksA Survey," *IEEE Commun. Surveys Tuts.*, vol. 24, no. 1, pp. 306–345, 2022.

[5] F. Liu, Y. Cui, C. Masouros, J. Xu, T. X. Han, Y. C. Eldar, and S. Buzzi, "Integrated Sensing and Communications: Toward Dual-Functional Wireless Networks for 6G and Beyond," *IEEE J. Sel. Areas Commun.*, vol. 40, no. 6, pp. 1728–1767, 2022.

[6] F. Liu, C. Masouros, A. Li, T. Ratnarajah, and J. Zhou, "MIMO Radar and Cellular Coexistence: A Power-Efficient Approach Enabled by Interference Exploitation," *IEEE Trans. Signal Process.*, vol. 66, no. 14, pp. 3681–3695, 2018.

[7] K. V. Mishra, M. Bhavani Shankar, V. Koivunen, B. Ottersten, and S. A. Vorobyov, "Toward Millimeter-Wave Joint Radar Communications: A Signal Processing Perspective," *IEEE Signal Process. Mag.*, vol. 36, no. 5, pp. 100–114, 2019.

[8] D. Ma, N. Shlezinger, T. Huang, Y. Liu, and Y. C. Eldar, "Joint Radar-Communication Strategies for Autonomous Vehicles: Combining Two Key Automotive Technologies," *IEEE Signal Process. Mag.*, vol. 37, no. 4, pp. 85–97, 2020.

[9] J. A. Zhang, F. Liu, C. Masouros, R. W. Heath, Z. Feng, L. Zheng, and A. Petropulu, "An Overview of Signal Processing Techniques for Joint Communication and Radar Sensing," *IEEE J. Sel. Topics Signal Process.*, vol. 15, no. 6, pp. 1295–1315, 2021.

[10] L. Zheng, M. Lops, and X. Wang, "Adaptive Interference Removal for Uncoordinated Radar/Communication Coexistence," *IEEE J. Sel. Topics Signal Process.*, vol. 12, no. 1, pp. 45–60, 2018.

[11] J. Qian, M. Lops, L. Zheng, X. Wang, and Z. He, "Joint System Design for Coexistence of MIMO Radar and MIMO Communication," *IEEE Trans. Signal Process.*, vol. 66, no. 13, pp. 3504–3519, 2018.

[12] B. Tang, H. Wang, L. Qin, and L. Li, "Waveform Design for Dual-function MIMO Radar-communication Systems," in *2020 IEEE 11th Sensor Array and Multichannel Signal Processing Workshop (SAM)*, Hangzhou, China, 2020, pp. 1–5.

[13] P. Kumari, S. A. Vorobyov, and R. W. Heath, "Adaptive Virtual Waveform Design for Millimeter-Wave Joint CommunicationRadar," *IEEE Trans. Signal Process.*, vol. 68, pp. 715–730, 2020.

[14] F. Liu, C. Masouros, T. Ratnarajah, and A. Petropulu, "On Range Sidelobe Reduction for Dual-Functional Radar-Communication Waveforms," *IEEE Wireless Commun. Lett.*, vol. 9, no. 9, pp. 1572–1576, 2020.

[15] F. Liu, L. Zhou, C. Masouros, A. Li, W. Luo, and A. Petropulu, "Toward Dual-functional Radar-Communication Systems: Optimal Waveform Design," *IEEE Trans. Signal Process.*, vol. 66, no. 16, pp. 4264–4279, 2018.

[16] X. Hu, C. Masouros, F. Liu, and R. Nissel, "MIMO-OFDM Dual-Functional Radar-Communication Systems: Low-PAPR Waveform Design," 2021. [Online]. Available: https://arxiv.org/abs/2109.13148.

[17] F. Liu, C. Masouros, A. Li, H. Sun, and L. Hanzo, "MU-MIMO Communications With MIMO Radar: From Co-Existence to Joint Transmission," *IEEE Trans. Wireless Commun.*, vol. 17, no. 4, pp. 2755–2770, 2018.

[18] Z. Cheng, B. Liao, and Z. He, "Hybrid Transceiver Design for Dual-Functional Radar-Communication System," in *2020 IEEE 11th Sensor Array and Multichannel Signal Processing Workshop (SAM)*, Hangzhou, China, 2020, pp. 1–5.

[19] W. Yuan, F. Liu, C. Masouros, J. Yuan, D. W. K. Ng, and N. Gonzlez-Prelcic, "Bayesian Predictive Beamforming for Vehicular Networks: A Low-Overhead Joint Radar-Communication Approach," *IEEE Trans. Wireless Commun.*, vol. 20, no. 3, pp. 1442–1456, 2021.

[20] C. Xu, B. Clerckx, and J. Zhang, "Multi-Antenna Joint Radar and Communications: Precoder Optimization and Weighted Sum-Rate vs Probing Power Tradeoff," *IEEE Access*, vol. 8, pp. 173 974–173 982, 2020.

[21] N. Su, F. Liu, and C. Masouros, "Secure Radar-Communication Systems With Malicious Targets: Integrating Radar, Communications and Jamming Functionalities," *IEEE Trans. Wireless Commun.*, vol. 20, no. 1, pp. 83–95, 2021.

[22] X. Liu, T. Huang, N. Shlezinger, Y. Liu, J. Zhou, and Y. C. Eldar, "Joint Transmit Beamforming for Multiuser MIMO Communications and MIMO Radar," *IEEE Trans. Signal Process.*, vol. 68, pp. 3929–3944, 2020.

[23] J. Li and P. Stoica, "MIMO Radar with Colocated Antennas," *IEEE Signal Process. Mag.*, vol. 24, no. 5, pp. 106–114, 2007.

[24] C. Masouros and E. Alsusa, "Dynamic linear precoding for the exploitation of known interference in MIMO broadcast systems," *IEEE Trans. Wireless Commun.*, vol. 8, no. 3, pp. 1396–1404, 2009.

[25] C. Masouros and G. Zheng, "Exploiting Known Interference as Green Signal Power for Downlink Beamforming Optimization," *IEEE Trans. Signal Process.*, vol. 63, no. 14, pp. 3628–3640, 2015.

[26] Y. Wang and A. Li, "ADMM Based Interference Exploitation Multi-User One-Bit Massive MIMO Precoding," *IEEE Trans. Veh. Technol.*, vol. 72, no. 7, pp. 9561–9566, 2023.

[27] M. Alodeh, D. Spano, A. Kalantari, C. G. Tsinos, D. Christopoulos, S. Chatzinotas, and B. Ottersten, "Symbol-Level and Multicast Precoding for Multiuser Multiantenna Downlink: A State-of-the-Art, Classification, and Challenges," *IEEE Commun. Surveys Tuts.*, vol. 20, no. 3, pp. 1733–1757, 2018.

[28] A. Li, D. Spano, J. Krivochiza, S. Domouchtsidis, C. G. Tsinos, C. Masouros, S. Chatzinotas, Y. Li, B. Vucetic, and B. Ottersten, "A Tutorial on Interference Exploitation via Symbol-Level Precoding: Overview, State-of-the-Art and Future Directions," *IEEE Commun. Surveys Tuts.*, vol. 22, no. 2, pp. 796–839, Mar. 2020.

[29] R. Liu, M. Li, Q. Liu, and A. L. Swindlehurst, "Dual-Functional Radar-Communication Waveform Design: A Symbol-Level Precoding Approach," *IEEE J. Sel. Topics Signal Process.*, vol. 15, no. 6, pp. 1316–1331, 2021.

[30] R. Liu, M. Li, Q. Liu, and A. L. Swindlehurst, "Joint Waveform and Filter Designs for STAP-SLP-Based MIMO-DFRC Systems," *IEEE J. Sel. Areas Commun.*, vol. 40, no. 6, pp. 1918–1931, 2022.

[31] P. Li, Z. Xiao, M. Li, R. Liu, and Q. Liu, "Low-Range-Sidelobe Waveform Design for MIMO-OFDM ISAC Systems," 2023. [Online]. Available: https://arxiv.org/abs/2305.18847.

[32] A. Li, C. Masouros, F. Liu, and A. L. Swindlehurst, "Massive MIMO 1-Bit DAC Transmission: A Low-Complexity Symbol Scaling Approach," *IEEE Trans. Wireless Commun.*, vol. 17, no. 11, pp. 7559–7575, Nov. 2018.

[33] A. Li, C. Masouros, B. Vucetic, Y. Li, and A. L. Swindlehurst, "Interference Exploitation Precoding for Multi-Level Modulations: Closed-Form Solutions," *IEEE Trans. Commun.*, vol. 69, no. 1, pp. 291–308, 2021.

[34] A. Li, C. Shen, X. Liao, C. Masouros, and A. L. Swindlehurst, "Practical Interference Exploitation Precoding Without Symbol-by-Symbol Optimization: A Block-Level Approach," *IEEE Trans. Wireless Commun.*, vol. 22, no. 6, pp. 3982–3996, 2023.

[35] P. Stoica, J. Li, and Y. Xie, "On Probing Signal Design For MIMO Radar," *IEEE Transactions on Signal Processing*, vol. 55, no. 8, pp. 4151–4161, 2007.

[36] L. Wu, B. Wang, Z. Cheng, B. S. M. R, and B. Ottersten, "Joint Symbol-Level Precoding and Sub-Block-Level RIS Design for Dual-Function Radar-Communications," in *2023 IEEE International Conference on Acoustics, Speech and Signal Processing (ICASSP)*, Rhodes Island, Greece, 2023, pp. 1–5.

[37] S. Boyd and L. Vandenberghe, *Convex Optimization*. Cambridge University Press, 2004.

[38] R. Liu, M. Li, Q. Liu, and A. L. Swindlehurst, "Secure Symbol-Level Precoding in MU-MISO Wiretap Systems," *IEEE Transactions on Information Forensics and Security*, vol. 15, pp. 3359–3373, 2020.

[39] K.-Y. Wang, A. M.-C. So, T.-H. Chang, W.-K. Ma, and C.-Y. Chi, "Outage Constrained Robust Transmit Optimization for Multiuser MISO Downlinks: Tractable Approximations by Conic Optimization," *IEEE Transactions on Signal Processing*, vol. 62, no. 21, pp. 5690–5705, 2014.

[40] P. Wolfe, "The Simplex Method for Quadratic Programming," *Econometrica*, vol. 27, no. 1, pp. 170–170, 1960.

[41] F. Alizadeh and D. Goldfarb, "Second-order cone programming," *Mathematical Programming*, vol. 95, no. 1, pp. 3–51, 2003.

[42] Y. Wang, Y. Wen, A. Li, X. Hu, and C. Masouros, "Block-Level Interference Exploitation Precoding for MU-MISO: An ADMM Approach," 2023. [Online]. Available: https://arxiv.org/abs/2308.12749.

Yiran Wang received the bachelors degree in communication engineering from Central South University in 2021. She is currently pursuing the Ph.D. degree with the School of Information and Communications Engineering, Faculty of Electronic and Information Engineering, Xian Jiaotong University. Her research interests include integrated sensing and communication, symbol-level precoding and optimizations.

Xiaoyan Hu (Member, IEEE) received the Ph.D. degree in Electronic and Electrical Engineering from University College London (UCL), London, U.K., in 2020. From 2019 to 2021, she was a Research Fellow with the Department of Electronic and Electrical Engineering, UCL, U.K. She is currently an Associate Professor with the School of Information and Communications Engineering, Xi'an Jiaotong University, Xi'an, China. Her research interests are in the areas of 5G&6G wireless communications, including topics such as edge computing, reconfigurable intelligent surface, UAV communications, integrated sensing and communications (ISAC), secure&covert communications, and learning-based communications. She is the recipient of the IEEE Communication Society Big Data 2023 Best Influential Paper Award. She has been recognized as an Exemplary Reviewer for IEEE COMMUNICATIONS LETTERS. From 2020 to 2023, she served as the Assistant to the Editor-in-Chief of IEEE WIRELESS COMMUNICATIONS LETTERS, and she is currently serving as an Associate Editor for IEEE WIRELESS COMMUNICATIONS LETTERS. She has also served as a Guest Editor for ELECTRONICS on Physical Layer Security and for CHINA COMMUNICATIONS Blue Ocean Forum on MAC and Networks.

Ang Li (Senior Member, IEEE) received his Ph.D. degree in the Communications and Information Systems research group, Department of Electrical and Electronic Engineering, University College London in April 2018. He was a postdoctoral research associate in the School of Electrical and Information Engineering, The University of Sydney from May 2018 to February 2020. He joined Xi'an Jiaotong University in March 2020 and is now a Professor in the School of Information and Communications Engineering, Faculty of Electronic and Information Engineering, Xian Jiaotong University, Xian, China. His main research interests lie in the physical-layer techniques in wireless communications, including MIMO/massive MIMO, interference exploitation, symbol-level precoding, and reconfigurable MIMO, etc. He currently serves as the Associate Editor for IEEE COMMUNICATIONS LETTERS, IEEE OPEN JOURNAL OF SIGNAL PROCESSING, and EURASIP JOURNAL ON WIRELESS COMMUNICATIONS AND NETWORKING. He is the recipient of the 2021 IEEE Signal Processing Society Young Author Best Paper Award. He has been an Exemplary Reviewer for IEEE COMMUNICATIONS LETTERS, IEEE TRANSACTIONS ON COMMUNICATIONS, and IEEE WIRELESS COMMUNICATIONS LETTERS. He has served as the Co-Chair of the IEEE ICASSP 2020 Special Session on 'Hardware-Efficient Large-Scale Antenna Arrays: The Stage for Symbol-Level Precoding', and has organized a Tutorial in IEEE ICC 2021 on 'Interference Exploitation through Symbol Level Precoding: Energy Efficient Transmission for 6G and Beyond'.

Christos Masouros (Fellow, IEEE) received the Diploma degree in electrical and computer engineering from the University of Patras, Greece, in 2004, and the M.Sc. (by research) and Ph.D. degrees in electrical and electronic engineering from The University of Manchester, U.K., in 2006 and 2009, respectively. In 2008, he was a Research Intern with Philips Research Labs, U.K. From 2009 to 2010, he was a Research Associate with The University of Manchester and a Research Fellow with Queen's University Belfast from 2010 to 2012. In 2012, he joined University College London, as a Lecturer. He has held a Royal Academy of Engineering Research Fellowship from 2011 to 2016. Since 2019, he has been a Full Professor of signal processing and wireless communications with the Information and Communication Engineering Research Group, Department of Electrical and Electronic Engineering, and affiliated with the Institute for Communications and Connected Systems, University College London. His research interests include wireless communications and signal processing with a particular focus on green communications, large-scale antenna systems, integrated sensing and communications (ISAC), interference mitigation techniques for MIMO, and multicarrier communications. He waw a co-recipient of the 2021 IEEE SPS Young Author Best Paper Award. He was a recipient of the Best Paper Award from IEEE GLOBECOM 2015 and IEEE WCNC 2019 conferences. He has been recognized as an Exemplary Editor for IEEE COMMUNICATIONS LETTERS and an Exemplary Reviewer for IEEE TRANSACTIONS ON COMMUNICATIONS. He is a founding member and the Vice-Chair of the IEEE Emerging Technology Initiative on ISAC, the Vice Chair of the IEEE Special Interest Group on ISAC, and the Chair of the IEEE Special Interest Group on Energy Harvesting Communication Networks. He is an Area Editor of IEEE TRANSACTIONS ON WIRELESS COMMUNICATIONS, and an Editor of IEEE TRANSACTIONS ON COMMUNICATIONS and IEEE OPEN JOURNAL OF SIGNAL PROCESSING, and the Editor-at-Large of IEEE OPEN JOURNAL OF THE COMMUNICATION SOCIETY. He was an Associate Editor of IEEE COMMUNICATIONS LETTERS and the Guest Editor for a number of special issues on IEEE JOURNAL OF SELECTED TOPICS IN SIGNAL PROCESSING and IEEE JOURNAL OF SELECTED AREAS IN COMMUNICATIONS.

Kai-Kit Wong (Fellow, IEEE) received the BEng, the MPhil, and the PhD degrees, all in Electrical and Electronic Engineering, from the Hong Kong University of Science and Technology, Hong Kong, in 1996, 1998, and 2001, respectively. After graduation, he took up academic and research positions at the University of Hong Kong, Lucent Technologies, Bell-Labs, Holmdel, the Smart Antennas Research Group of Stanford University, and the University of Hull, UK. He is currently the Chair of Wireless Communications with the Department of Electronic and Electrical Engineering, University College London, UK. His current research centers around 5G and beyond mobile communications, including topics such as massive MIMO, full-duplex communications, millimetre-wave communications, edge caching and fog networking, physical layer security, wireless power transfer and mobile computing, V2X communications, fluid antenna communications systems, and of course cognitive radios. He is a co-recipient of the 2013 IEEE Signal Processing Letters Best Paper Award and the 2000 IEEE VTS Japan Chapter Award at the IEEE Vehicular Technology Conference in Japan in 2000, and a few other international best paper awards. He is Fellow of IEEE and IET and is also on the editorial board of several international journals. He has served as Senior Editor for IEEE COMMUNICATIONS LETTERS since 2012 and also for IEEE WIRELESS COMMUNICATIONS LETTERS since 2016. He had also previously served as Associate Editor for IEEE SIGNAL PROCESSING LETTERS from 2009 to 2012 and Editor for IEEE TRANSACTIONS ON WIRELESS COMMUNICATIONS from 2005 to 2011. He was also Guest Editor for IEEE JSAC SI on virtual MIMO in 2013 and on physical layer security for 5G in 2018. He served as the Editor-in-Chief for IEEE WIRELESS COMMUNICATIONS LETTERS between 2020 and 2023.

Kun Yang (Fellow, IEEE) received his PhD from the Department of Electronic & Electrical Engineering of University College London (UCL), UK. He is currently a Chair Professor in the School of Computer Science & Electronic Engineering, University of Essex, UK, leading the Network Convergence Laboratory (NCL). He is also an affiliated professor of Nanjing University. His main research interests include wireless networks and communications, communication-computing cooperation, and new AI (artificial intelligence) for wireless. He has published 500+ papers and filed 50 patents. He serves on the editorial boards of a number of IEEE journals (e.g., IEEE WCM, TVT, TNB). He is a Deputy Editor-in-Chief of IET Smart Cities Journal. He has been a Judge of GSMA GLOMO Award at World Mobile Congress Barcelona since 2019. He was a Distinguished Lecturer of IEEE ComSoc (2020-2021) and a Recipient of the 2024 IET Achievement Medals and the winner of IEEE CommSoft TCs Technical Achievement Award 2024. He is a Member of Academia Europaea (MAE), a Fellow of IEEE, a Fellow of IET and a Distinguished Member of ACM.